1. PŘÍLOHA 1

1.1. Přepočet REF hodnot z protimeteru na objemovou vlhkost

Na studovaném materiálu z lokality STR (sublokalita F1) byla provedena kalibrace pro přepočet REF hodnot z protimeteru na objemovou vlhkost pískovce. Jádro pískovce o m_{pf} = 180 g bylo nejprve saturováno destilovanou vodou. Saturace spočívala v ponoření jádra po dobu 24 hodin do nádoby zaplněné 50 cm sloupcem destilované vody. Po vyjmutí jádra z vody a okapání (5 s po vyjmutí) bylo jádro znovu zváženo a hodnota byla zapsána jako m_s (=205,9 g).

Modifikací rovnice (4.1), kdy za m_p bylo dosazeno m_s, byla vypočítána hmotnostní vlhkost jádra po saturaci θ_h (12,5 hm. %) a obdobně byla podle rovnice (4.2) vypočítána i objemová vlhkost θ po saturaci (25,1 obj. %). Následně byla pomocí protimeteru v náhodných místech po celém povrchu pískovcového jádra změřena série 10 REF hodnot. Jako výsledná hodnota byla uvažována vždy nejvyšší naměřená hodnota REF, jak doporučuje výrobce protimeteru ve svém manuálu (Greisinger electronic GmbH, 2008). Nejvyšší naměřená hodnota byla během kalibrace o 6 až 21 % vyšší než průměrná hodnota naměřené sady (tab. P1.1).

Tab. P1.1. Naměřené REF hodnoty z protimeteru v jednotlivých sadách měření pro příslušné objemové vlhkosti θ (obj. %). Uvedeny jsou maximální a průměrné REF hodnoty a procentuální rozdíl mezi nimi.

θ (obj. %)	**25,1**	**18,4**	**12,8**	**11,3**	**10,6**	**9,2**	**8,5**	**8,2**
REF	24	23	22	21	20	16	13	11
	25	24	21	22	19	19	14	11
	22	23	22	22	20	17	14	10
	26	24	23	21	19	15	11	8
	24	22	21	21	21	19	12	9
	23	23	23	20	21	16	15	10
	25	23	24	19	20	14	14	12
	26	21	22	20	19	16	11	12
	23	22	21	20	19	21	14	14
	23	25	23	21	20	18	13	13
max REF hodnota	**26**	**25**	**24**	**22**	**21**	**21**	**15**	**14**
průměrná REF hodnota	**24,1**	**23**	**22,2**	**20,7**	**19,8**	**17,1**	**13,1**	**11**
rozdíl mezi průměrnou a max REF hodnotou	**7 %**	**8 %**	**8 %**	**6 %**	**6 %**	**19 %**	**13 %**	**21 %**

Po změření REF hodnot bylo jádro ponecháno vypařovat v podmínkách relativní vlhkosti vzduchu ~40 % a teploty ~25 °C a průběžně byla zjišťována jeho aktuální hmotnost, dokud se po přepočtu podle rovnic (4.1 a 4.2) nesnížila objemová vlhkost jádra na další požadovanou hodnotu (změny v řádu desetin obj. procent až prvních obj. procent). Po snížení objemové vlhkosti na požadovanou hodnotu bylo jádro umístěno do dvou PVC víček, přičemž obě PVC víčka byla k sobě spojena svými horními podstavami pomocí silně utahované el. pásky, znemožňující významný únik vodní páry (Slavík, 2014). Jádro bylo takto ponecháno po dobu nejméně 96 hodin za účelem prostorově rovnoměrného přeuspořádání vlhkosti uvnitř jádra. Poté bylo jádro z PVC víček vyňato, zváženo (nová hmotnost byla označena jako aktuální m_p) a znovu byla pomocí protimeteru změřena série 10 REF hodnot.

Tímto způsobem bylo provedeno celkově 9 měření, přičemž poslední je vztaženo k hmotnosti m_{pf}, odpovídající hmotnosti jádra po vysoušení při teplotě 110 °C po dobu 48 hodin. Objemová vlhkost θ byla v tomto případě tedy rovna 0 % (podle rovnice 4.2). Nejvyšším naměřeným REF hodnotám z protimeteru byla vždy přiřazena patřičná objemová vlhkost. Tyto párové hodnoty jsou uvedeny v tab. P1.2. Vztah mezi nimi je popsatelný pomocí lineární funkce (P1.1; obr. P1.1), ve které x reprezentuje naměřenou maximální REF hodnotu a y reprezentuje příslušnou objemovou vlhkost.

Tab. P1.2. Výstup z kalibrace protimeteru. Párové hodnoty maximální REF hodnoty (-) z protimeteru a příslušné objemové vlhkosti θ (obj. %).

max REF hodnota (-)	26	25	24	22	21	21	15	14	4
θ (obj. %)	25,1	18,4	12,8	11,3	10,6	9,2	8,5	8,2	0,0

$$y = 0{,}7423x - 2{,}3566 \qquad \text{(P1.1)}$$

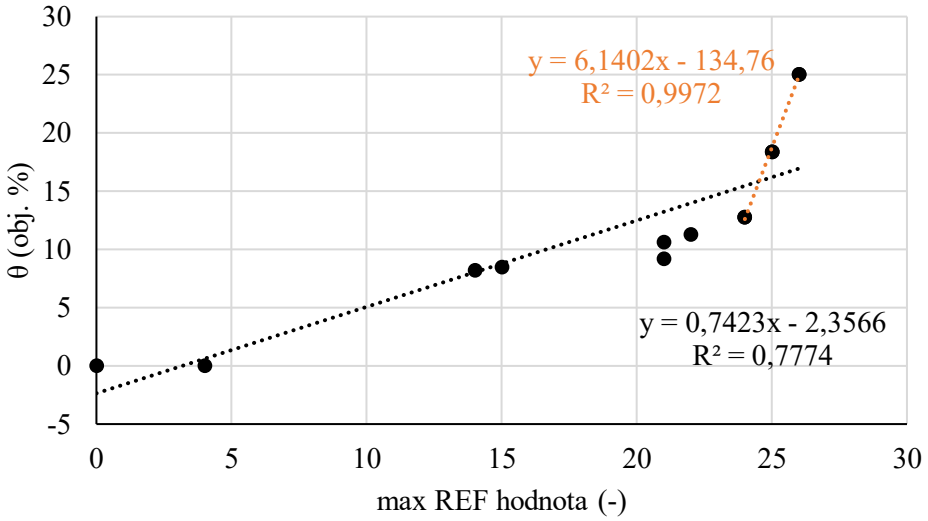

Obr. P1.1. Lineární funkce vyjadřující vztah mezi maximální REF hodnotou (-) z protimeteru a příslušnou objemovou vlhkostí θ (obj. %) podle kalibrace. Pro výpočty byla používána rovnice označená černou barvou (spodní).

Nejistoty v kalibraci lze spatřovat v nižší míře korelace (R^2 = 0,78) mezi naměřenými REF hodnotami a vypočítanými objemovými vlhkostmi, což může být způsobeno nerovnoměrně rozprostřenou vlhkostí uvnitř jádra (i přes snahu tomu zabránit) či nepřesným měřením.

Z grafu na obr. P.1 je patrné, že pro hodnoty REF ≥ 24 poslední tři měření leží na přímce s jinou směrnicí (y = 6,1402x - 134,76; vyjádřená oranžovou barvu), než která popisuje vztah v rozsahu celého měření. Po přepočtu podle obou rovnic se pro hodnotu REF = 24 liší výsledná hodnota objemové vlhkosti o 2 %. To je značný rozdíl, a protože jsou navíc hodnoty REF nad 24 spíše výjimečné, je výhodnější pro přepočet používat výhradně rovnici (P1.1). Po odmyšlení bodu REF = 26, který je od lineární funkce dané rovnicí (P1.1) nejvíce vzdálen a může se jednat o chybu měření, není navíc odlišná směrnice již v grafu tak zřejmá.

1.2. Dlouhodobá měření relativní vlhkosti vzduchu a teploty na lokalitách ML1, ML2, MA, DR

Na grafech obr. P1.2 až obr. P1.5 je uveden záznam z čidel měřících teplotu a relativní vlhkost vzduchu. Na obr. P1.6 je znázorněno rozložení srážek do jednotlivých měsíců v průběhu let 2005 až 2017 pro lokality ML1 a ML2.

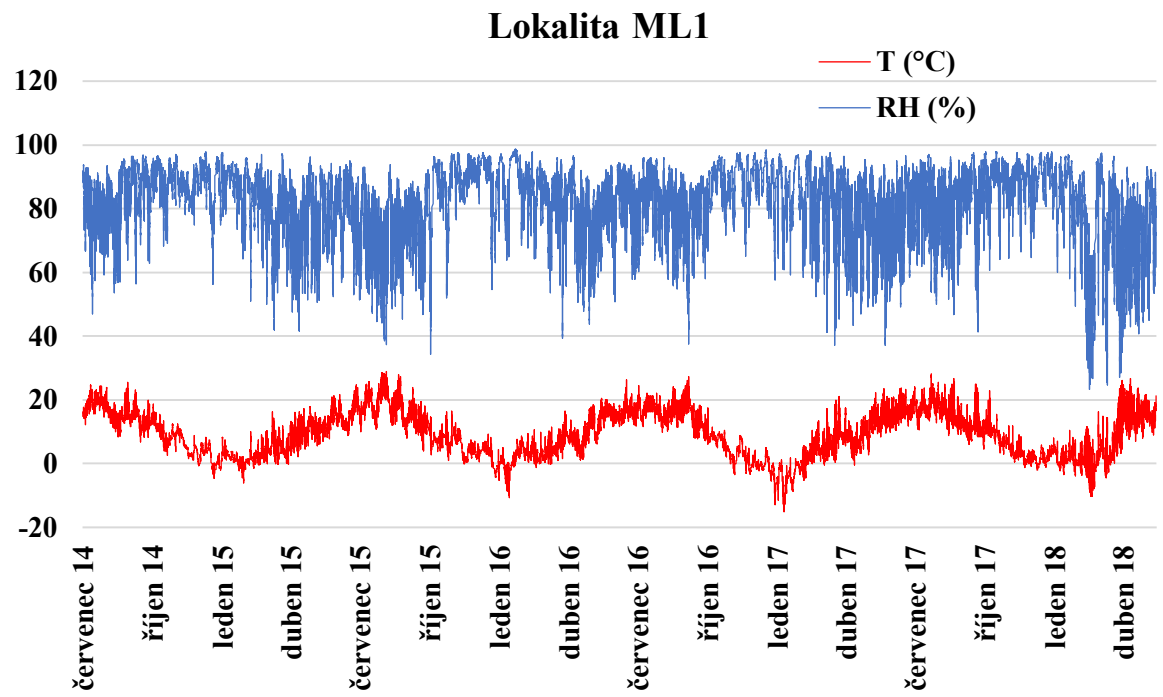

Obr. P1.2. Záznam relativní vlhkosti vzduchu (RH) a teploty (T) na lokalitě ML1 od července 2014 do května 2018.

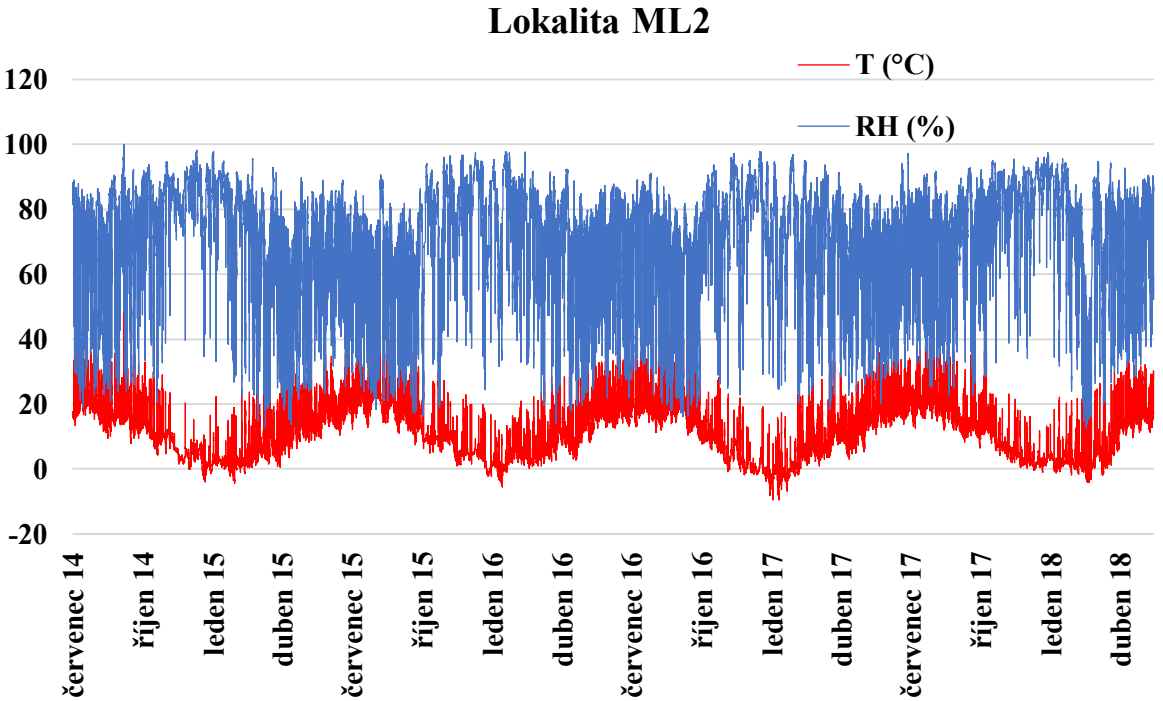

Obr. P1.3. Záznam relativní vlhkosti vzduchu (RH) a teploty (T) na lokalitě ML2 od července 2014 do května 2018.

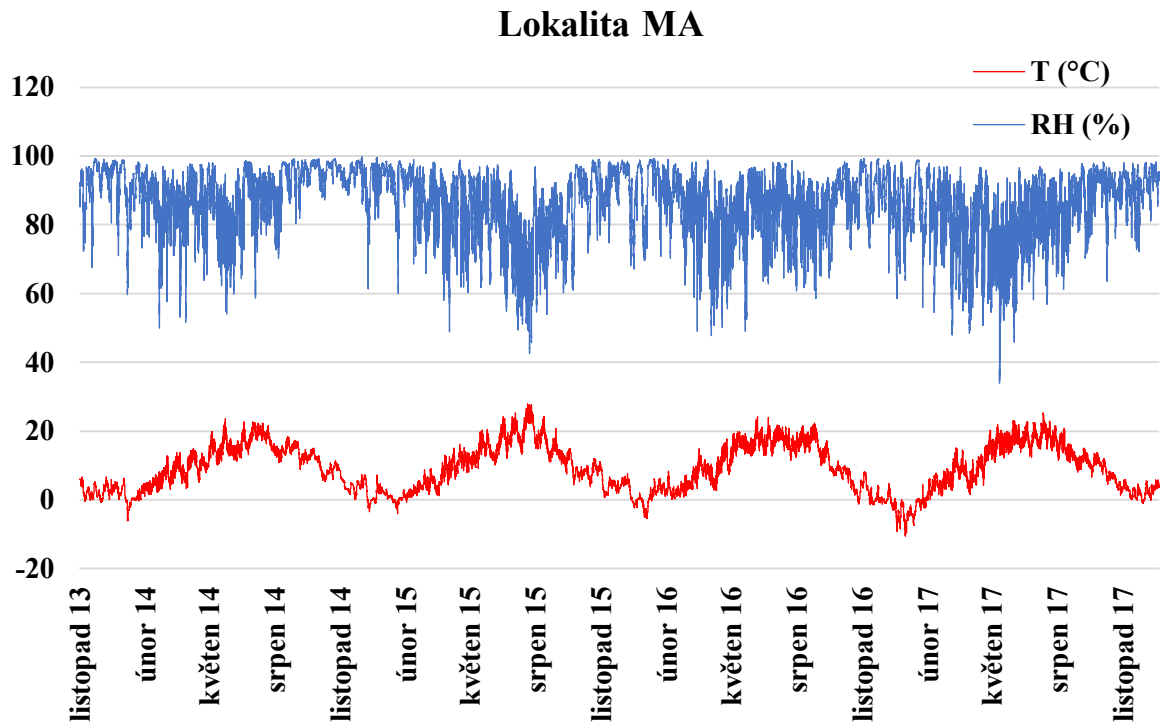

Obr. P1.4. Záznam relativní vlhkosti vzduchu (RH) a teploty (T) na lokalitě MA od listopadu 2013 do ledna 2018.

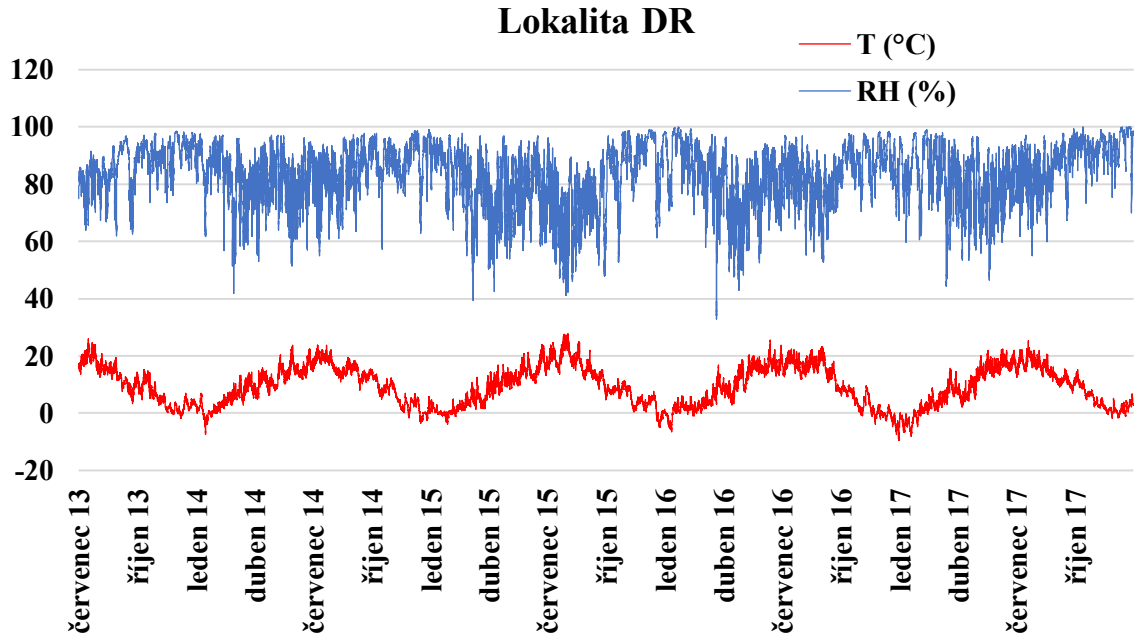

Obr. P1.5. Záznam relativní vlhkosti vzduchu (RH) a teploty (T) na lokalitě DR od července 2013 do ledna 2018.

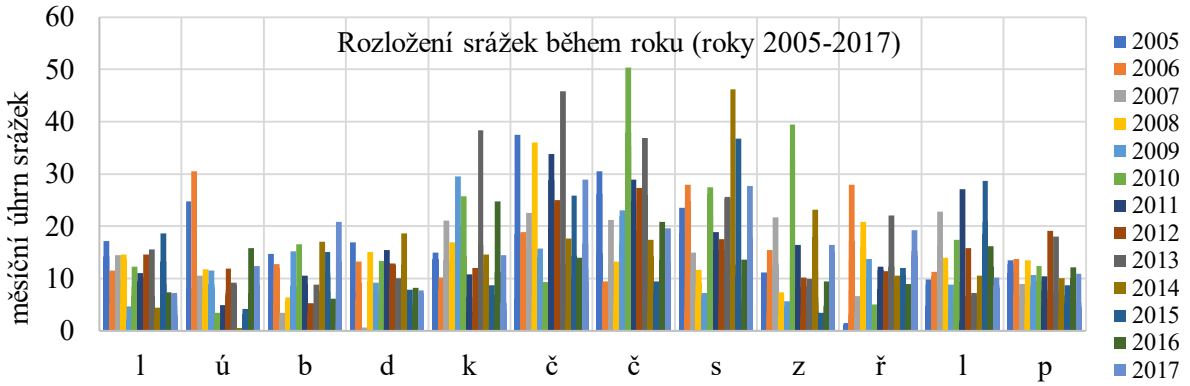

Obr. P1.6. Rozložení srážek do jednotlivých měsíců v průběhu let 2005 až 2017 pro lokality ML1 a ML2 (stanice Holenice). Zdroj: Český hydrometeorologický ústav.

1.3. Měření rychlosti proudění vzduchu pomocí automatických anemometrů

Na obr. P1.7 a obr. P1.8 jsou uvedeny časové řady měření rychlosti proudění vzduchu na lokalitě ML1 pomocí automatických anemometrů. Odečet hodnot probíhal každých 5 minut.

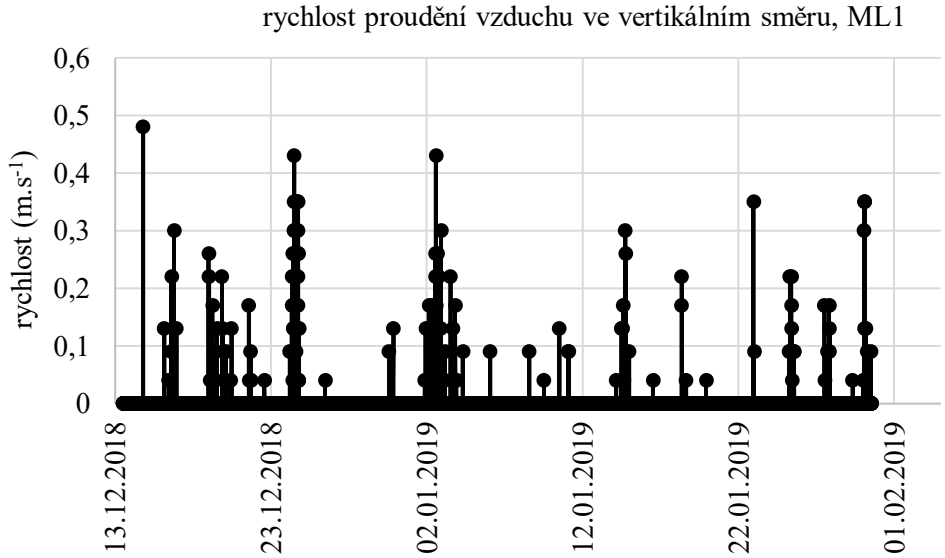

P1.7. Časová řada měření rychlosti proudění vzduchu ve vertikálním směru pomocí anemometru na lokalitě ML1.

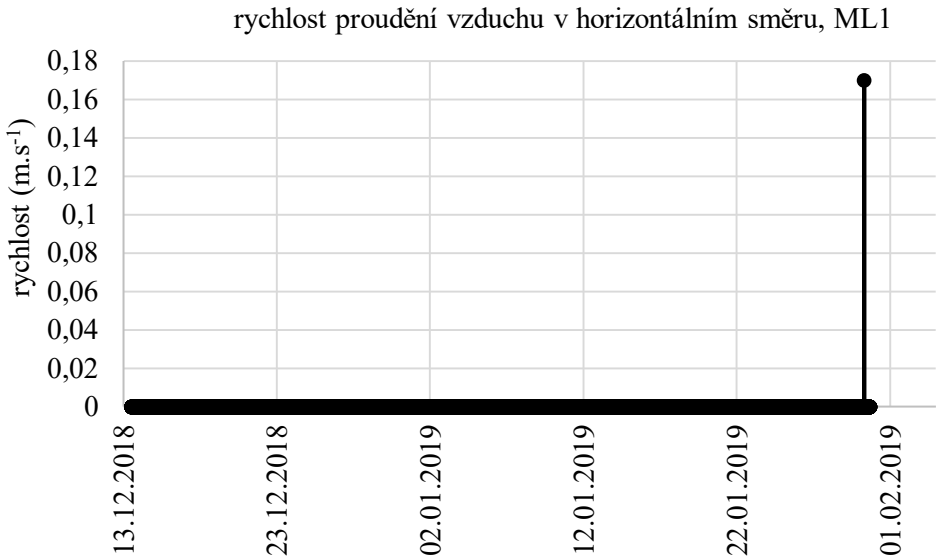

P1.8. Časová řada měření rychlosti proudění vzduchu v horizontálním směru pomocí anemometru na lokalitě ML1.

1.4. Dlouhodobá měření objemové vlhkosti a sacího tlaku na studovaných lokalitách

Na obr. P1.9 až obr. P1.14 jsou uvedeny grafy měření sacího tlaku pomocí mikrotensometrů a měření objemové vlhkosti pomocí TDR pro sublokality ML1 voštiny, ML2 hladká, ML2 voštiny, DR voštiny, DR převis a DR u stromu.

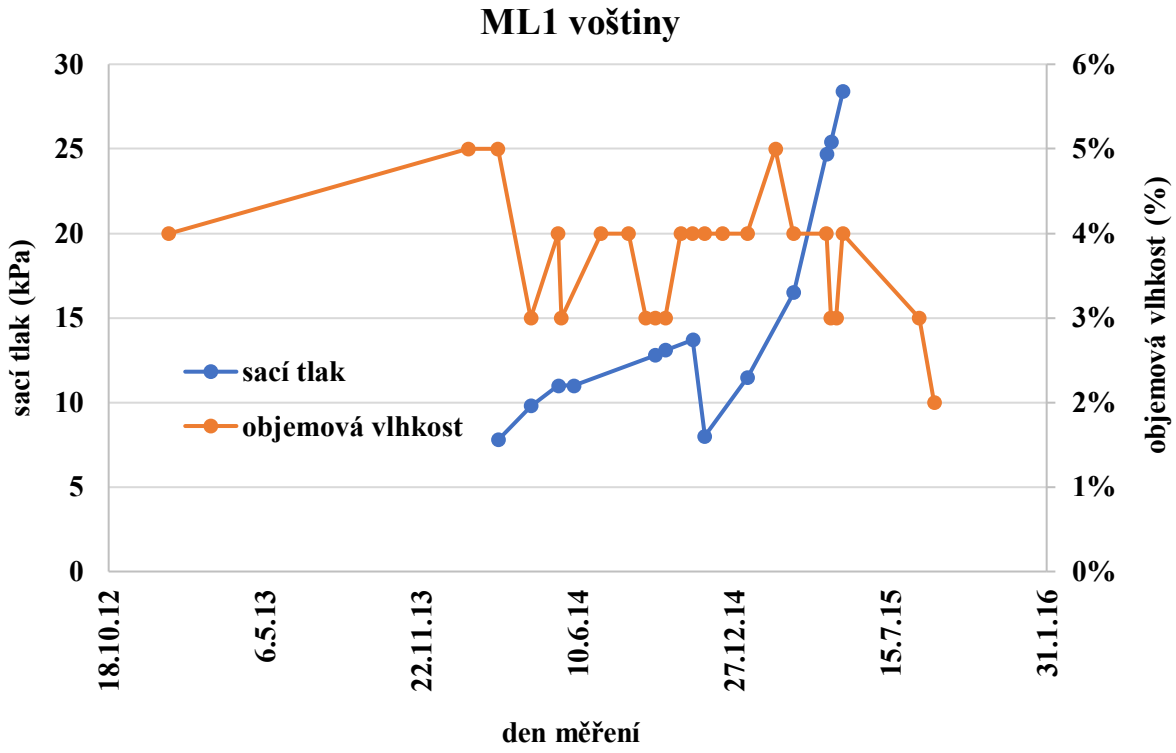

Obr. P1.9. Dlouhodobé měření sacího tlaku a objemové vlhkosti (TDR) na sublokalitě ML1 voštiny.

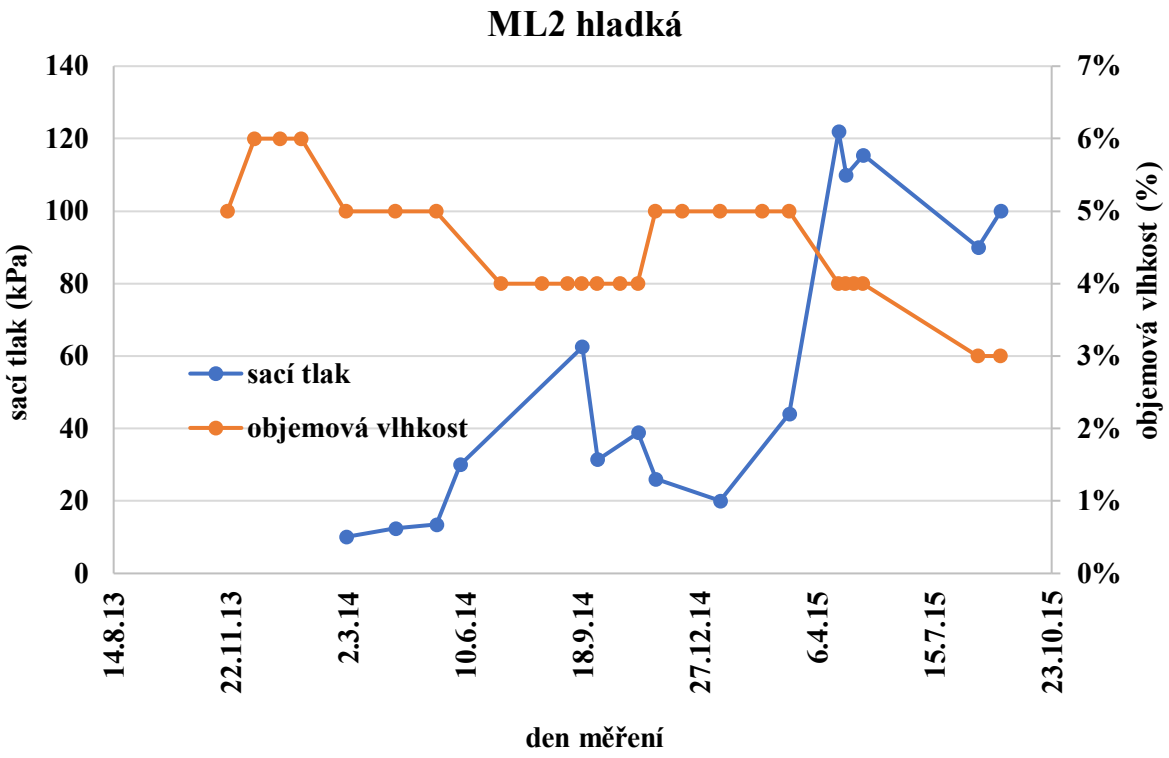

P1.10. Dlouhodobé měření sacího tlaku a objemové vlhkosti (TDR) na sublokalitě ML2 hladká.

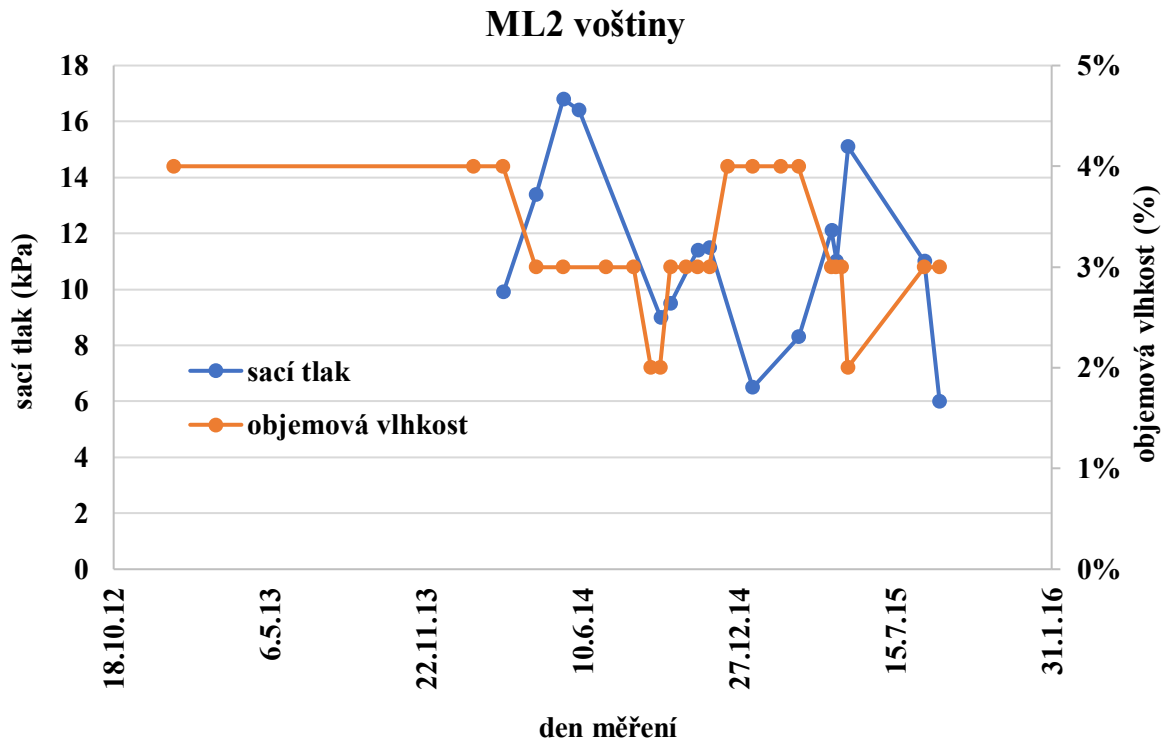

P1.11. Dlouhodobé měření sacího tlaku a objemové vlhkosti (TDR) na sublokalitě ML2 voštiny.

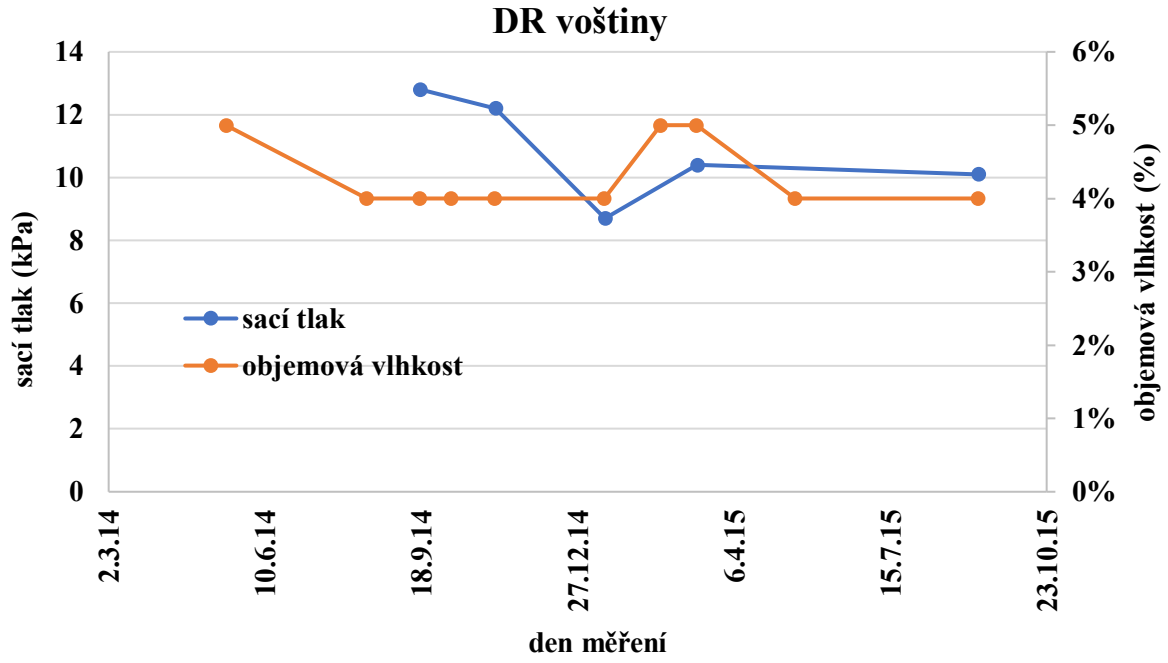

P1.12. Dlouhodobé měření sacího tlaku a objemové vlhkosti (TDR) na sublokalitě DR voštiny.

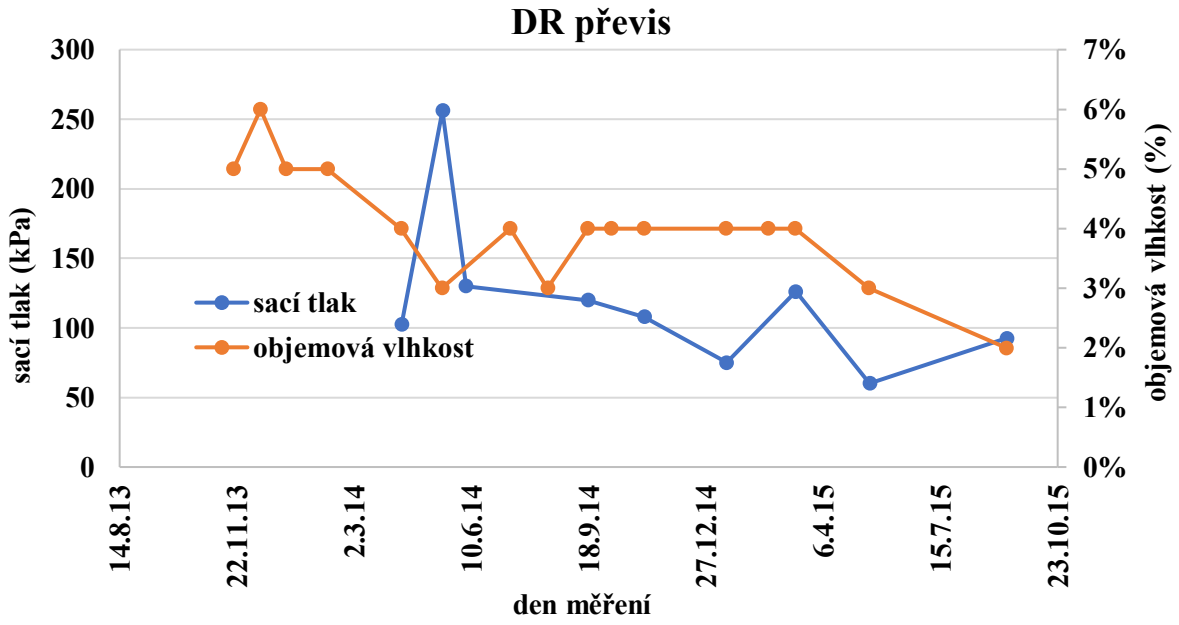

P1.13. Dlouhodobé měření sacího tlaku a objemové vlhkosti (TDR) na sublokalitě DR převis.

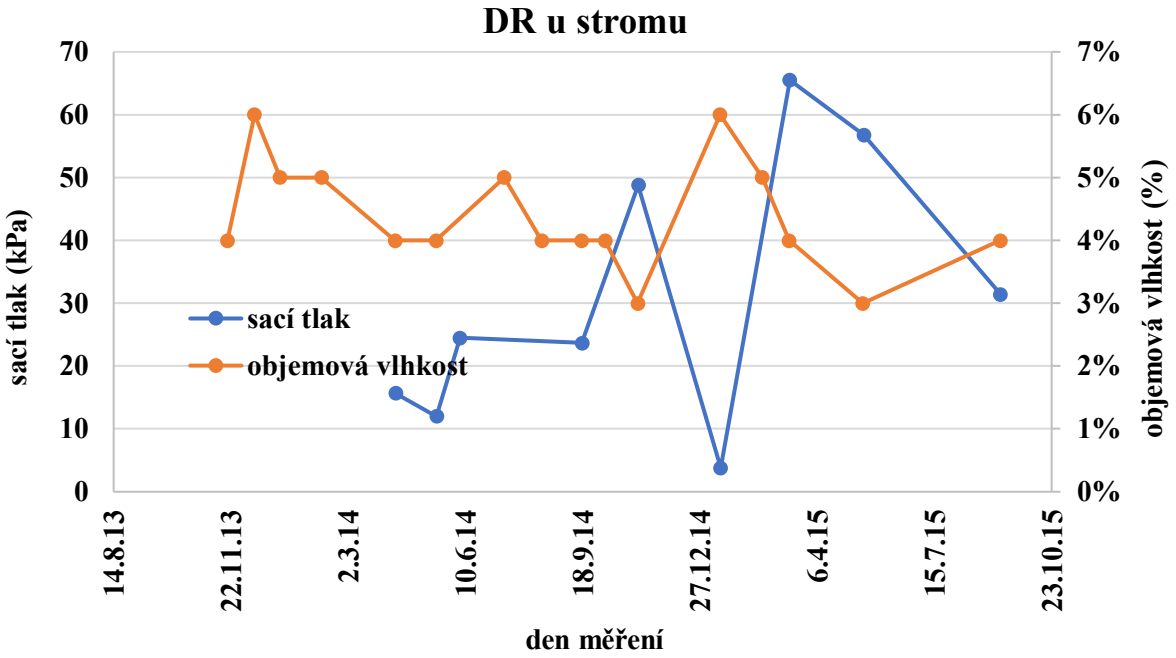

P1.14. Dlouhodobé měření sacího tlaku a objemové vlhkosti (TDR) na sublokalitě DR u stromu.

1.5. Časové řady relativní vlhkosti pískovcových povrchů naměřené pomocí protimeteru

Na obr. P1.15 až P1.19 jsou uvedeny časové řady měření relativní vlhkosti pískovcových povrchů naměřené pomocí protimeteru.

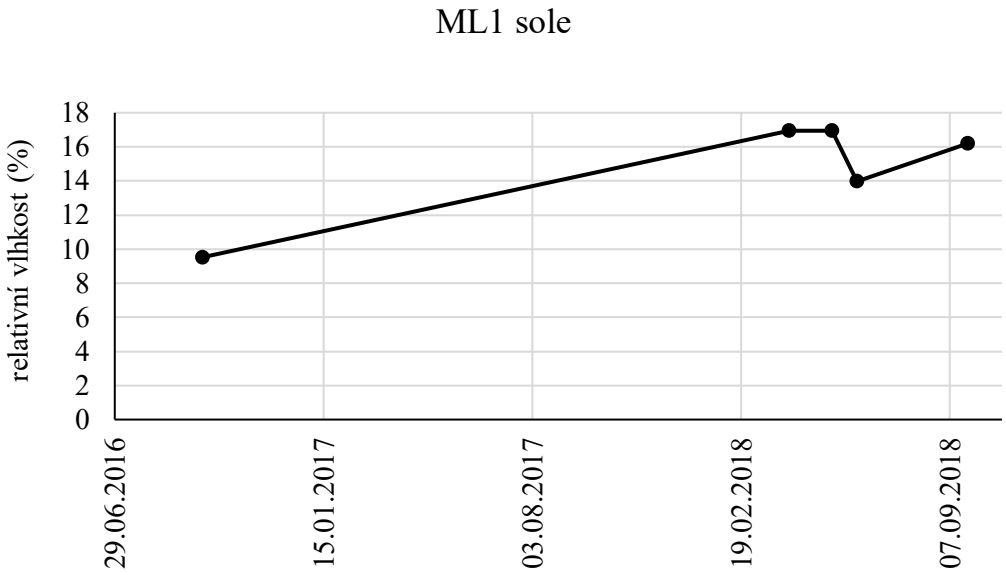

P1.15. Časová řada měření relativní vlhkosti povrchu pomocí protimeteru na sublokalitě ML1 sole.

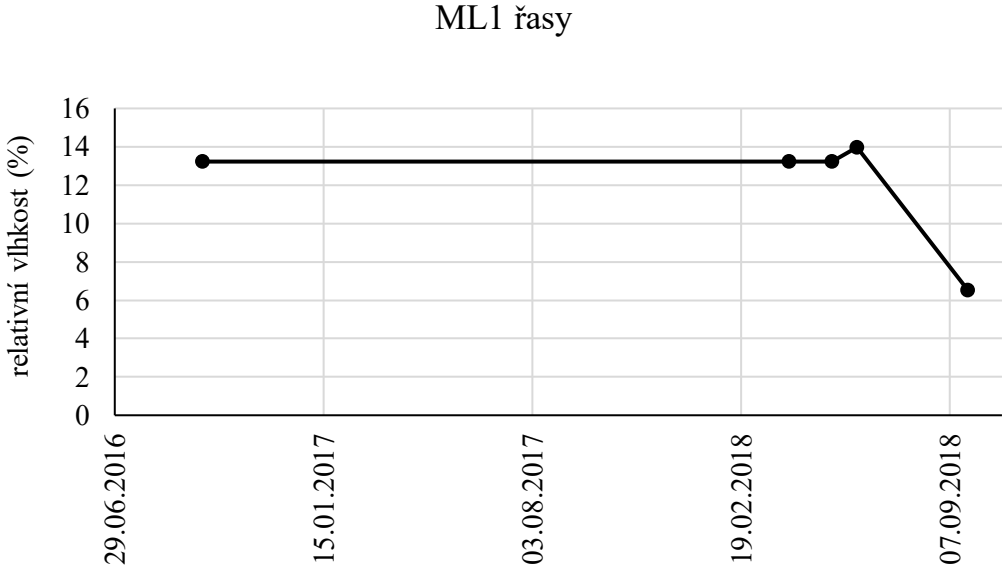

P1.16. Časová řada měření relativní vlhkosti povrchu pomocí protimeteru na sublokalitě ML1 řasy.

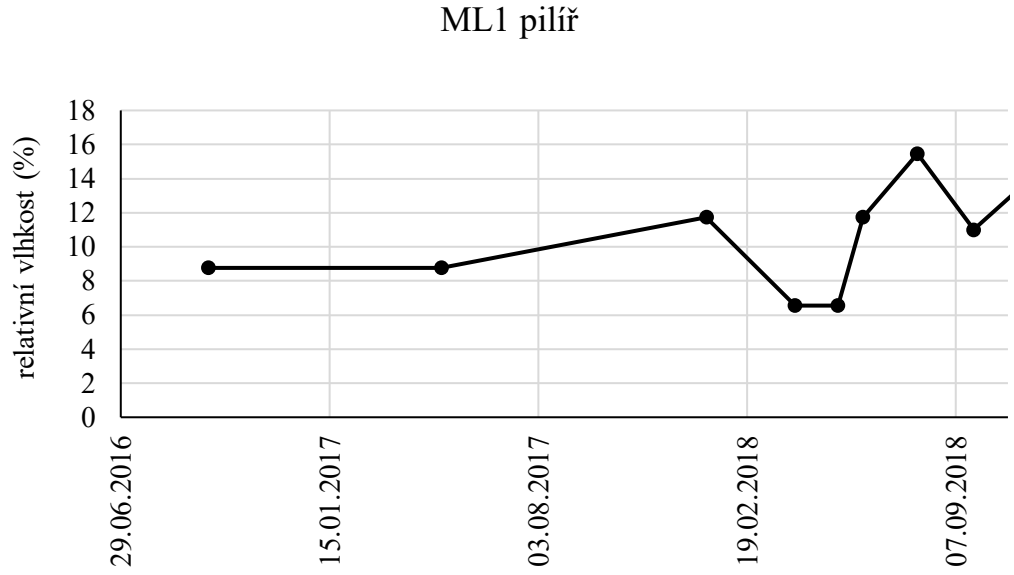

P1.17. Časová řada měření relativní vlhkosti povrchu pomocí protimeteru na sublokalitě ML1 pilíř.

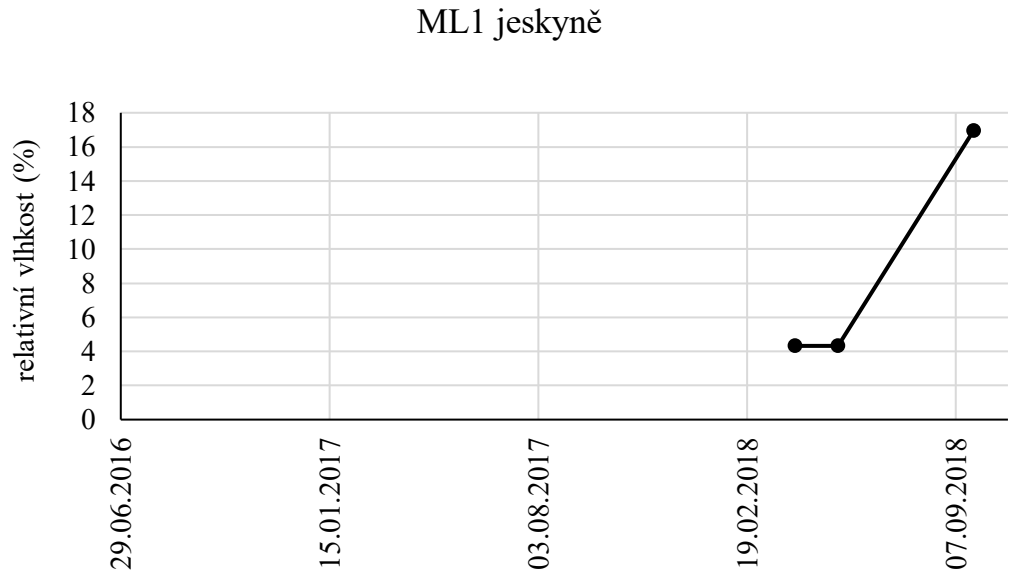

P1.18. Časová řada měření relativní vlhkosti povrchu pomocí protimeteru na sublokalitě ML1 jeskyně.

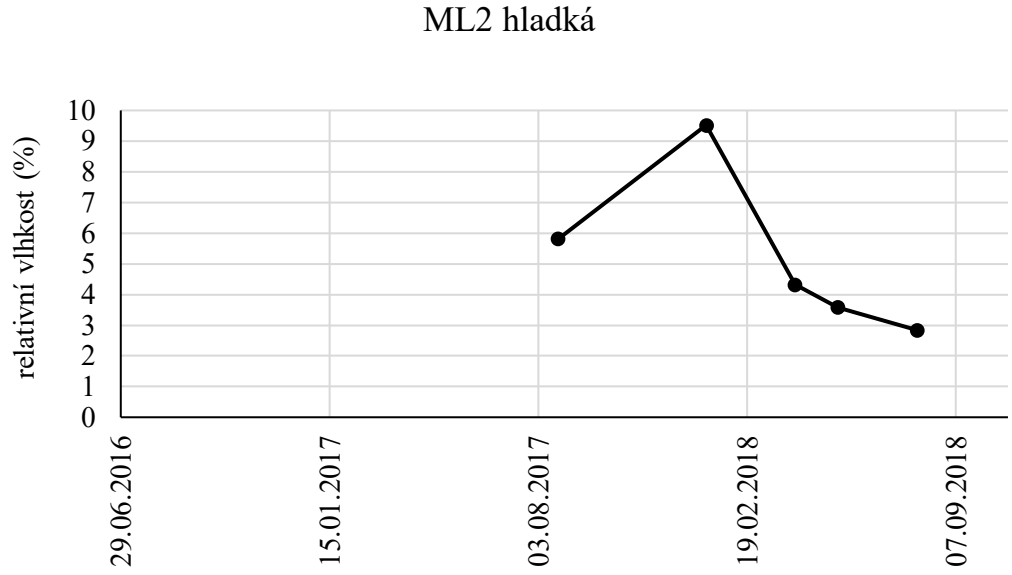

P1.19. Časová řada měření relativní vlhkosti povrchu pomocí protimeteru na sublokalitě ML2 hladká.

2. PŘÍLOHA 2

2.1. Srovnání měřené a vypočítané intenzity výparu

V kapitole 6.5 hlavní práce jsou uvedeny tabulky vypočítaných a naměřených hodnot intenzity výparu dohromady pro všechna měření na daných lokalitách. Zde v Příloze 2 jsou tabulky tab. P2.1 až tab. P2.3, ve kterých jsou uvedené hodnoty vztaženy taktéž k jednotlivým měřením. Vliv ochrany výparových aparátů před prouděním vzduchu a slunečním zářením na velikost relativní chyby je uveden v tab. P2.4.

Tab. P2.1. Vypočítané a naměřené hodoty intenzity výparu na lokalitě Budova 1. Uvedena je minimální, maximální a průměrná odchylka od měření (rozdíl mezi měřením a výpočtem) v $mm.rok^{-1}$ a relativní chyba výpočtů v procentech pro všechna měření. Kladné hodnoty odchylky od měření značí nadhodnocený výpočet oproti měření, záporné hodnoty podhodnocený výpočet oproti měření. T – teplota; RH – relativní vlhkost vzduchu; n – počet měřených období.

lokalita, typ a název výparového aparátu	**vypočítaný průměr za všechna období $mm.rok^{-1}$ (n)**	**změřený průměr za všechna období $mm.rok^{-1}$**	**minimální odchylka od měření $mm.rok^{-1}$ (relativní chyba %)**	**maximální odchylka od měření $mm.rok^{-1}$ (relativní chyba %)**	**průměrná T a RH pro všechna měřená období**
Budova 1, dry core A	5,8 (20)	15,8	-13 (38 %)	-16 (96 %)	9 °C, 80 %
Budova 1, dry core C	5,3 (20)	11,7	-1 (33 %)	-6 (91 %)	9 °C, 80 %
Budova 1, dry core E	9,9 (6)	32,5	-26 (57 %)	-26 (88 %)	14 °C, 70 %
Budova 1, dry core G	27,1 (6)	37,4	-3 (14 %)	-7 (47 %)	15 °C, 67 %
Budova 1, dry core H	6,4 (6)	16,6	-2 (46 %)	-18 (67 %)	15 °C, 67 %
Budova 1, dry core 12/13	10,0 (19)	14,5	-1 (6 %)	-5 (82 %)	9 °C, 79 %
Budova 1, dry core 12/14	7,1 (17)	12,9	+1 (8 %)	-10 (94 %)	10 °C, 77 %
Budova 1, dry core 12/16	8,2 (20)	29,2	-5 (57 %)	-11 (95 %)	9 °C, 80 %

Tab. P2.2. Vypočítané a naměřené hodoty intenzity výparu na lokalitě Budova 2. Uvedena je minimální, maximální a průměrná odchylka od měření (rozdíl mezi měřením a výpočtem) v $mm.rok^{-1}$ a relativní chyba výpočtů v procentech pro všechna měření. Kladné hodnoty odchylky od měření značí nadhodnocený výpočet oproti měření, záporné hodnoty podhodnocený výpočet oproti měření. T – teplota; RH – relativní vlhkost vzduchu; n – počet měřených období.

lokalita, typ a název výparového aparátu	**vypočítaný průměr za všechna období $mm.rok^{-1}$ (n)**	**změřený průměr za všechna období $mm.rok^{-1}$**	**minimální odchylka od měření $mm.rok^{-1}$ (%)**	**maximální odchylka od měření $mm.rok^{-1}$ (%)**	**průměrná T a RH pro všechna měřená období**
Budova 2, wet core PPPA	2350,1 (9)	2081,0	-40 (2 %)	+467 (46 %)	22 °C, 43 %
Budova 2, wet core PPPB	2350,1 (9)	2372,6	-7 (< 1 %)	+502 (51 %)	22 °C, 43 %

Tab. P2.3. Vypočítané a naměřené hodoty intenzity výparu na lokalitách Chorvatsko a Jordánsko. Uvedena je minimální, maximální a průměrná odchylka od měření (rozdíl mezi měřením a výpočtem) v $mm.rok^{-1}$ a relativní chyba výpočtů v procentech pro všechna měření. Kladné hodnoty odchylky od měření značí nadhodnocený výpočet oproti měření, záporné hodnoty podhodnocený výpočet oproti měření. T – teplota; RH – relativní vlhkost vzduchu; n – počet měřených období.

lokalita, typ a název výparového aparátu	**vypočítaný průměr za všechna období $mm.rok^{-1}$ (n)**	**změřený průměr za všechna období $mm.rok^{-1}$**	**minimální odchylka od měření $mm.rok^{-1}$ (%)**	**maximální odchylka od měření $mm.rok^{-1}$ (%)**	**průměrná T a RH pro všechna měřená období**
Chorvatsko, dry core A	86,4 (2)	108,8	-8 (10 %)	-37 (27 %)	37 °C, 41 %
Chorvatsko, dry core 12/13	128,4 (2)	155,8	+1 (1 %)	-56 (27 %)	37 °C, 41 %
Chorvatsko, dry core 12/16	109,6 (2)	107,5	-62 (41 %)	+66 (103 %)	37 °C, 41 %
Chorvatsko, wet core B	5616,9 (2)	5344,7	-455 (9 %)	+999 (18 %)	37 °C, 41 %
Jordánsko, dry core A	45,8 (3)	77,1	-12 (21 %)	-43 (46 %)	27 °C, 33 %
Jordánsko, wet core B	2979,2 (3)	3292,9	+20 (1 %)	-800 (22 %)	27 °C, 33 %

V kapitole 6.5 v hlavní práci jsou uvedeny jen některé grafy srovnávající měřené a vypočítané hodnoty intenzity výparu z výparových aparátů dry core a wet core. V Příloze 2 jsou zde uvedeny zbývající grafy pro dry core (obr. P2.1 až obr. P2.7) a wet core (obr. P2.6).

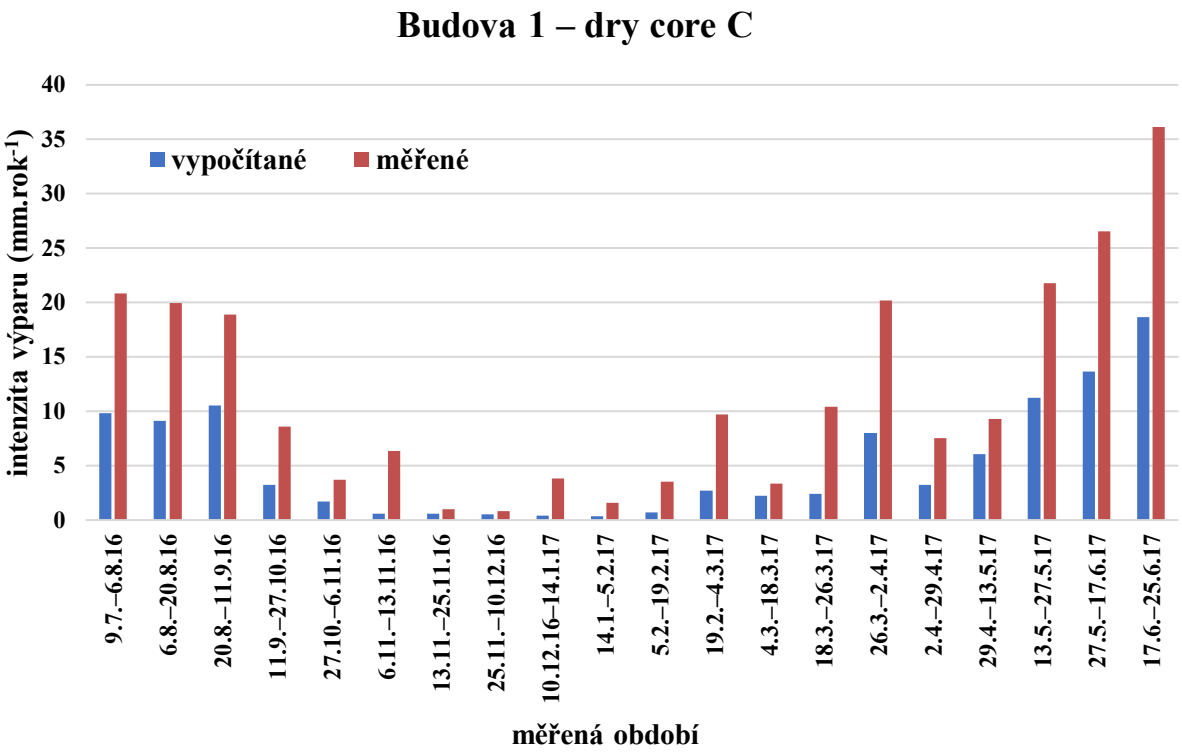

Obr. P2.1. Vypočítané a měřené hodnoty intenzity výparu pro jednotlivá měřená období na lokalitě Budova 1, výparový aparát dry core C.

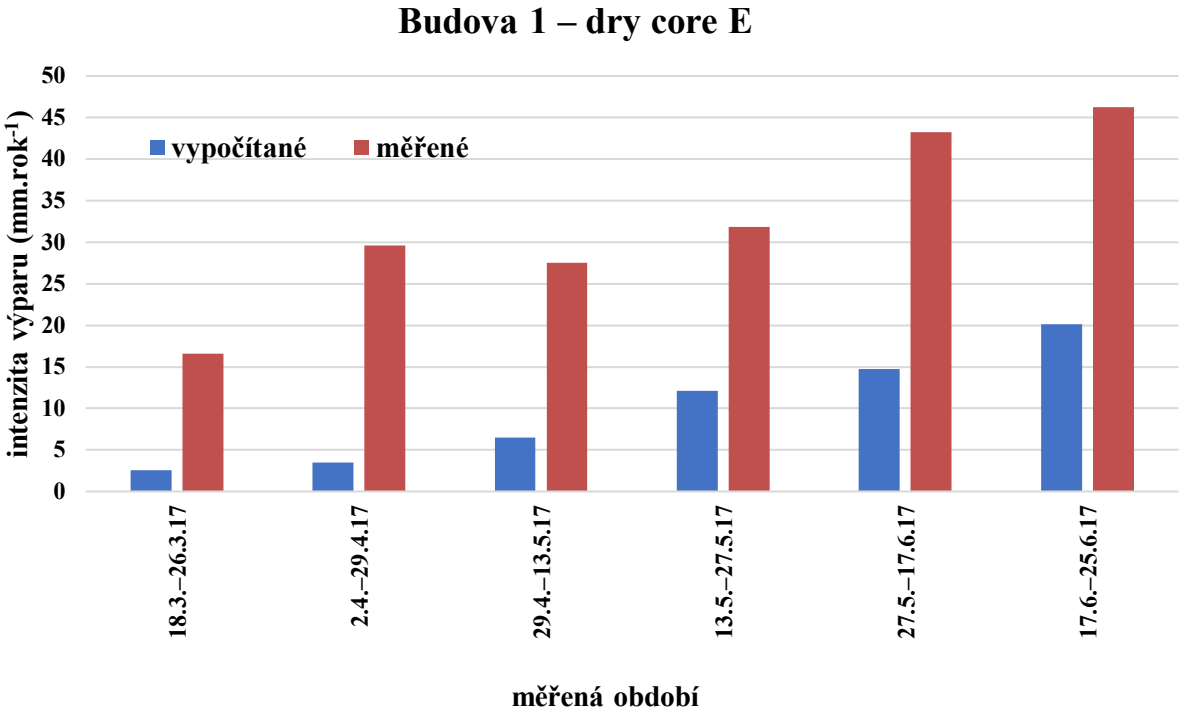

Obr. P2.2. Vypočítané a měřené hodnoty intenzity výparu pro jednotlivá měřená období na lokalitě Budova 1, výparový aparát dry core E.

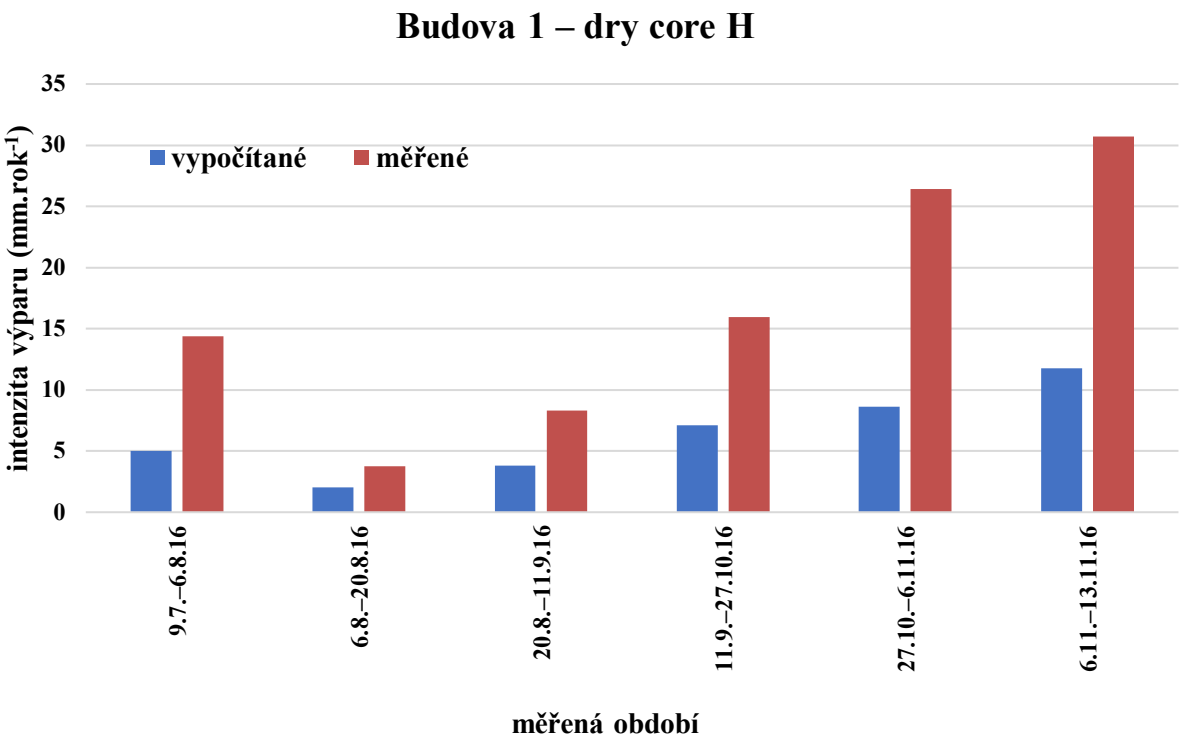

Obr. P2.3. Vypočítané a měřené hodnoty intenzity výparu pro jednotlivá měřená období na lokalitě Budova 1, výparový aparát dry core H.

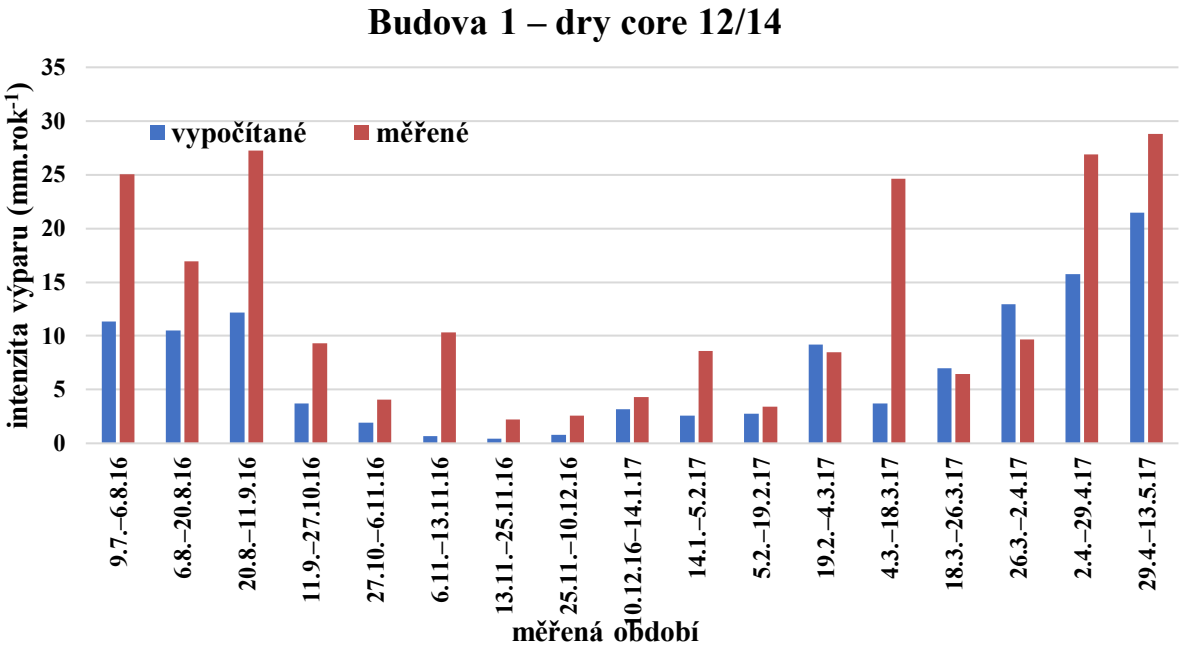

Obr. P2.4. Vypočítané a měřené hodnoty intenzity výparu pro jednotlivá měřená období na lokalitě Budova 1, výparový aparát dry core 12/14.

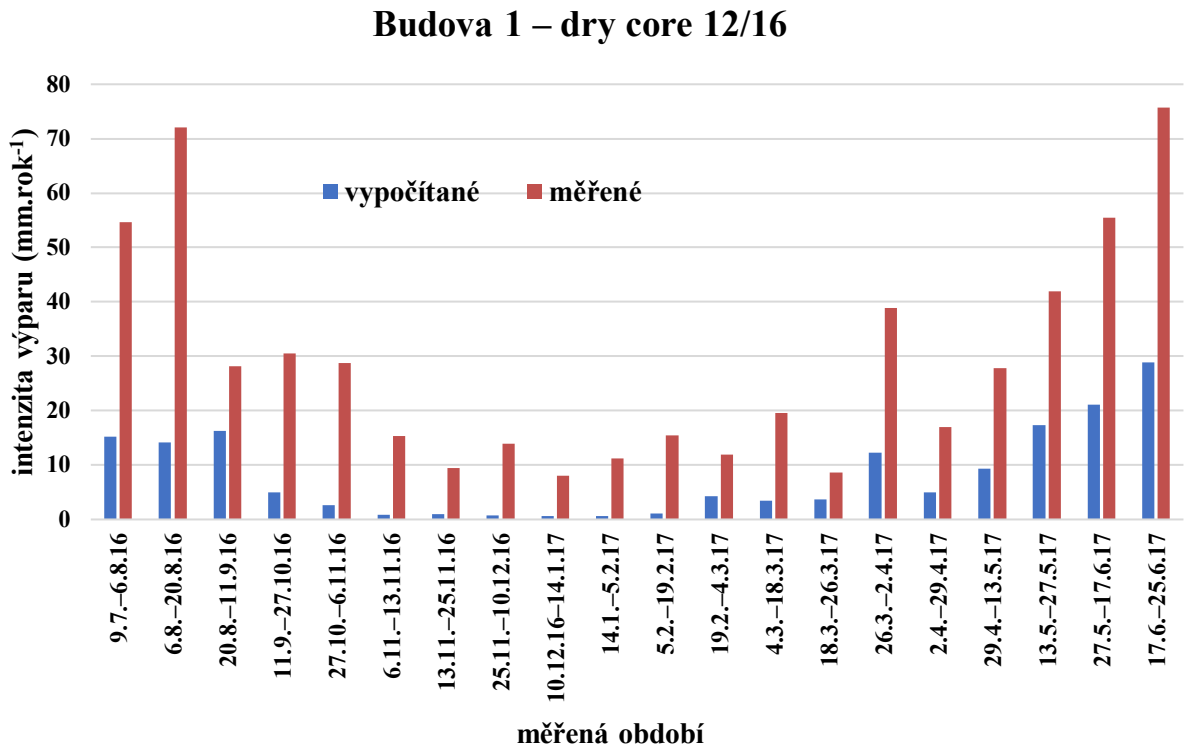

Obr. P2.5. Vypočítané a měřené hodnoty intenzity výparu pro jednotlivá měřená období na lokalitě Budova 1, výparový aparát dry core 12/16.

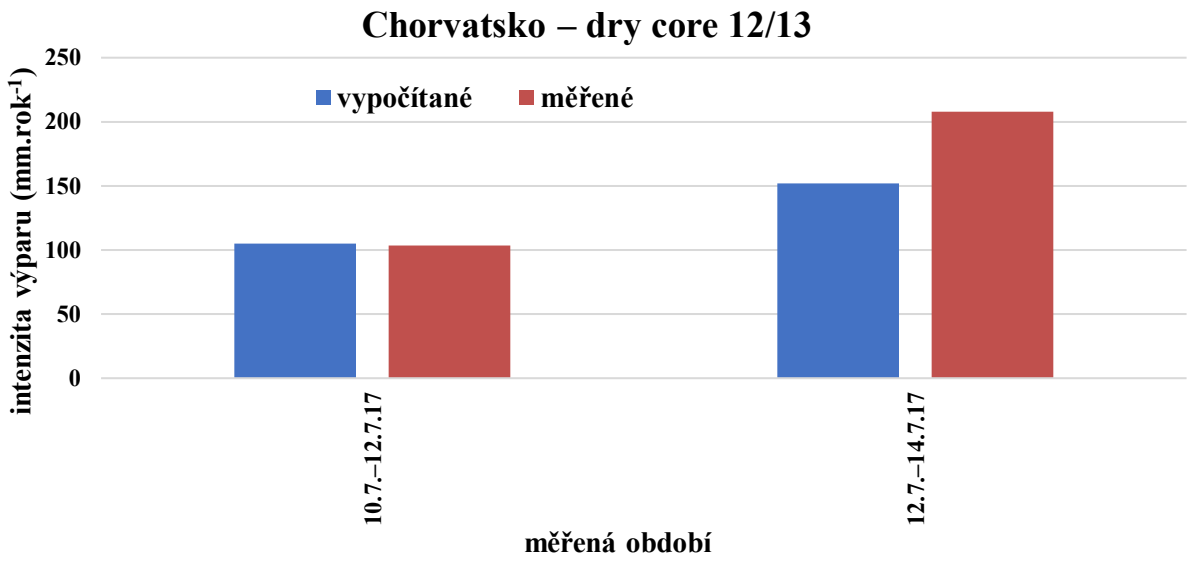

Obr. P2.6. Vypočítané a měřené hodnoty intenzity výparu pro jednotlivá měřená období na lokalitě Chorvatsko, výparový aparát dry core 12/13.

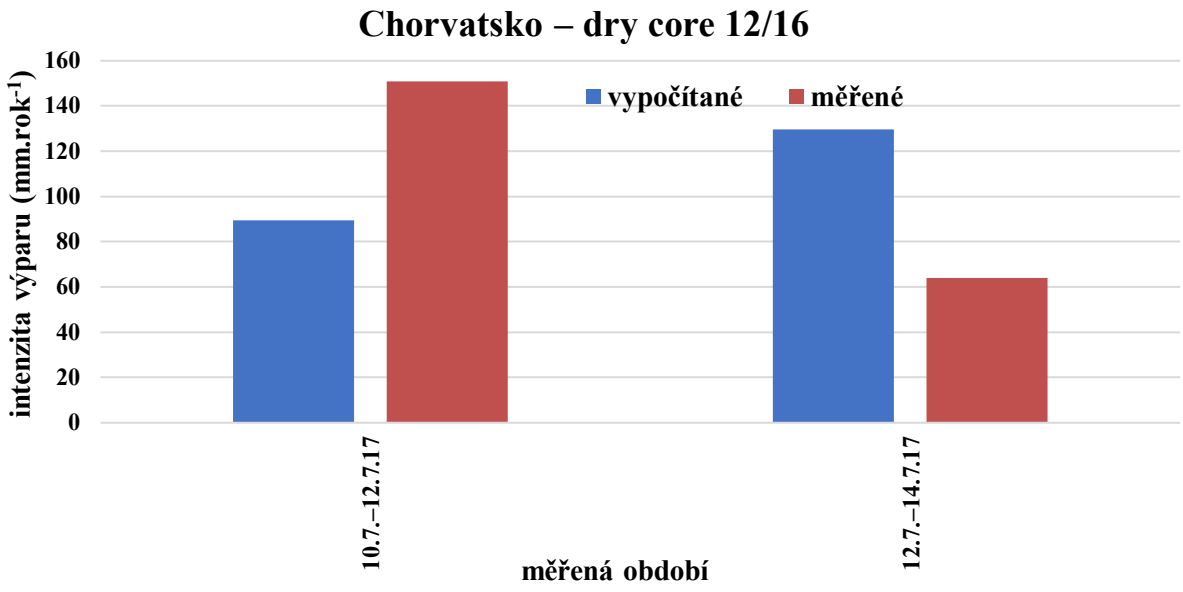

Obr. P2.7. Vypočítané a měřené hodnoty intenzity výparu pro jednotlivá měřená období na lokalitě Chorvatsko, výparový aparát dry core 12/16.

Tab. P2.4. Vliv ochrany výparových aparátů před prouděním vzduchu a slunečním zářením na velikost relativní chyby.

dry core	**ano**	**ne**	**částečně**
měření chráněná před větrem? relativní chyba	Jordánsko A 38 % (3)	Chorvatsko A, 12/13, 12/16 38 % (10)	vše Budova 1 58 % (114)
měření chráněná před sluncem? relativní chyba	Jordánsko A, Budova 1 12/13, 12/14, C, G, H 47 % (71)	Chorvatsko A, 12/13, 12/16, Budova 1 E 51 % (16)	Budova 1 12/16, A 73 % (40)
měření orientovaná k S relativní chyba	Budova 1 12/13, 12/14, C, G, H 48 % (68)		
měření orientovaná k J relativní chyba	Budova 1 12/16, A, E, Chorvatsko A, 12/13, 12/16 66 % (56)		
wet core	**ano**	**ne**	**částečně**
měření chráněná před větrem? relativní chyba	Jordánsko B 9 % (3)	Chorvatsko B, Budova 2 PPPA, PPPB 14 % (20)	
měření chráněná před sluncem? relativní chyba	Jordánsko B, Budova 2 PPPA, PPPB 13 % (21)	Chorvatsko B 13 % (2)	

2.2. Grafy měření rychlosti kapilárního nasákávání v laboratoři

Pod obrázky obr. P2.8 až obr. P2.11 jsou uvedeny grafy znázorňující průběh kapilárního nasákávání v čase měřeného v laboratoři skrz podloží a skrz biogenní skalní kůru pro vzorky z jednotlivých sublokalit v lomu Střeleč (lokalita STR).

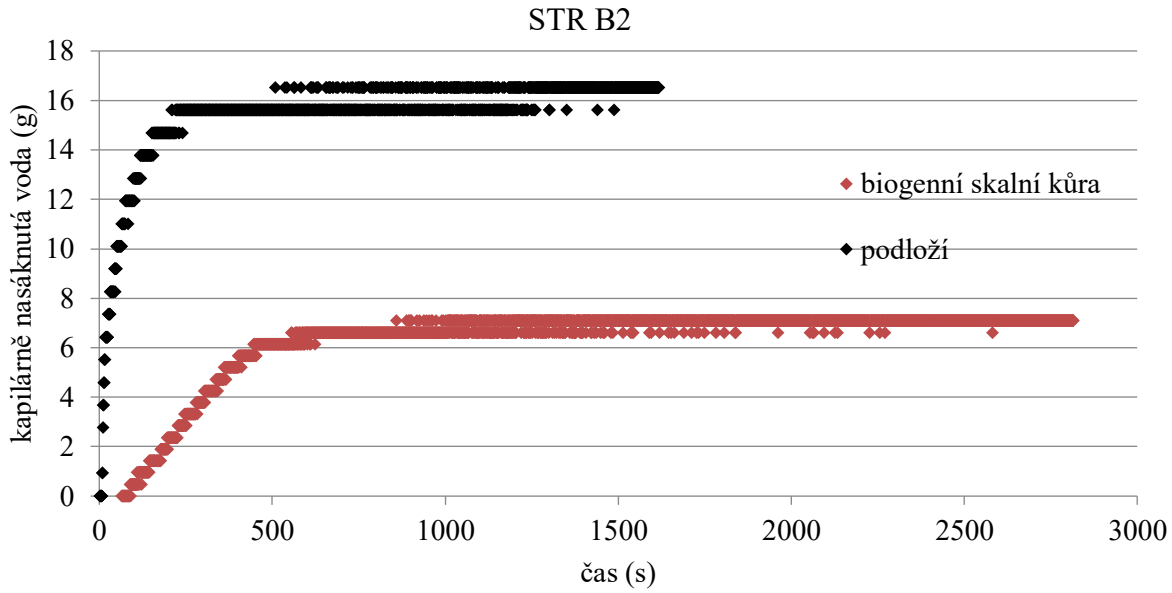

Obr. P2.8. Měření rychlosti kapilárního nasákávání pro vzorek ze sublokality STR B2.

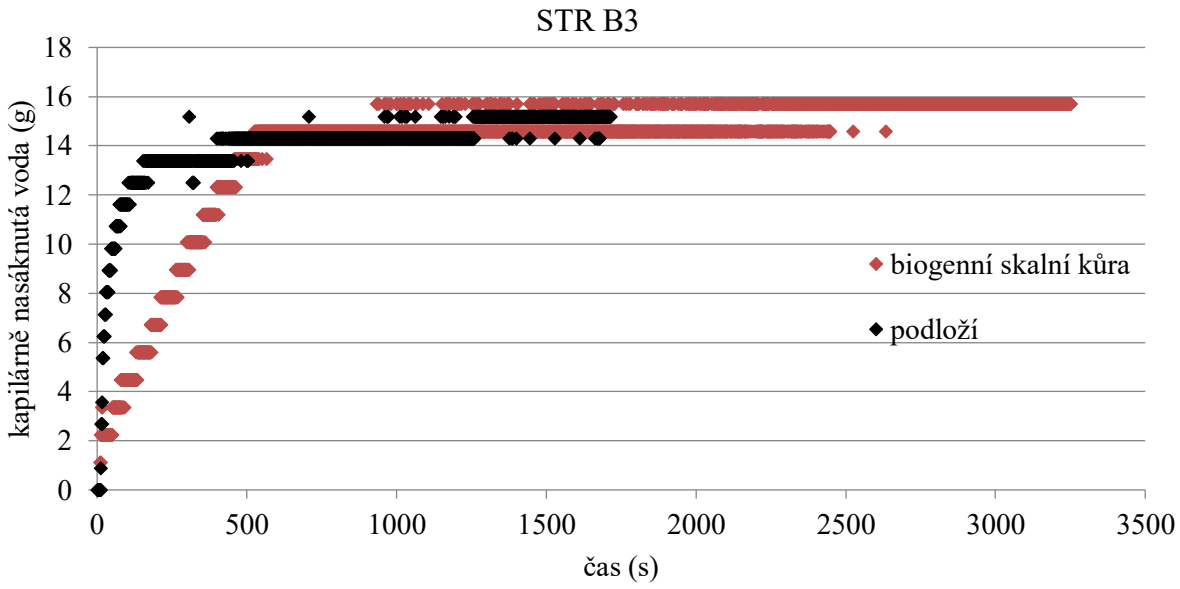

Obr. P2.9. Měření rychlosti kapilárního nasákávání pro vzorek ze sublokality STR B3.

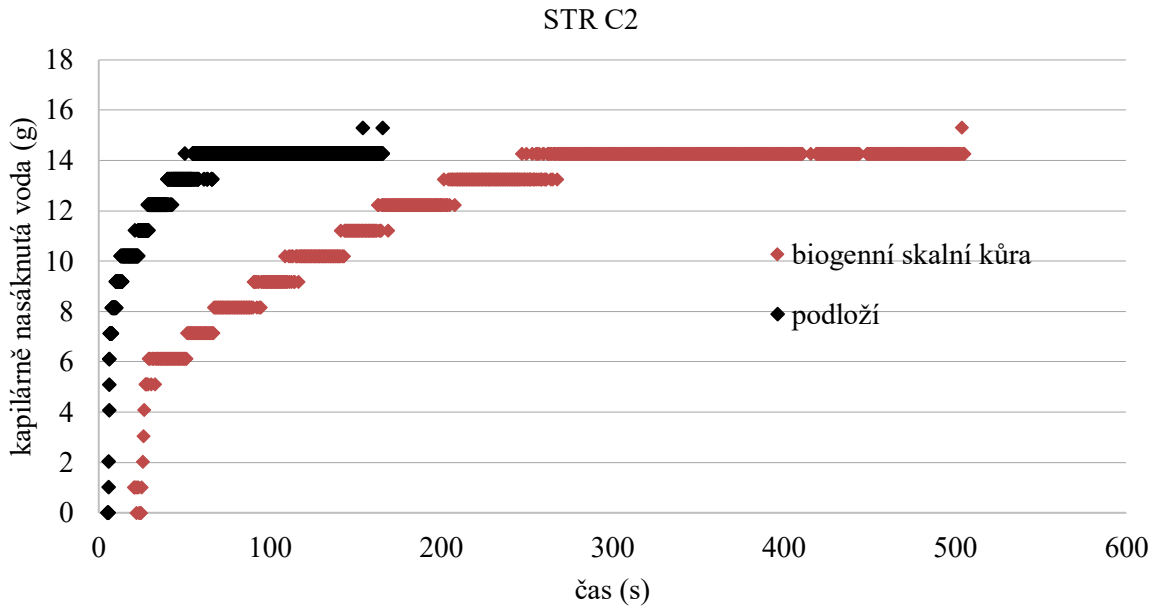

Obr. P2.10. Měření rychlosti kapilárního nasákávání pro vzorek ze sublokality STR C2.

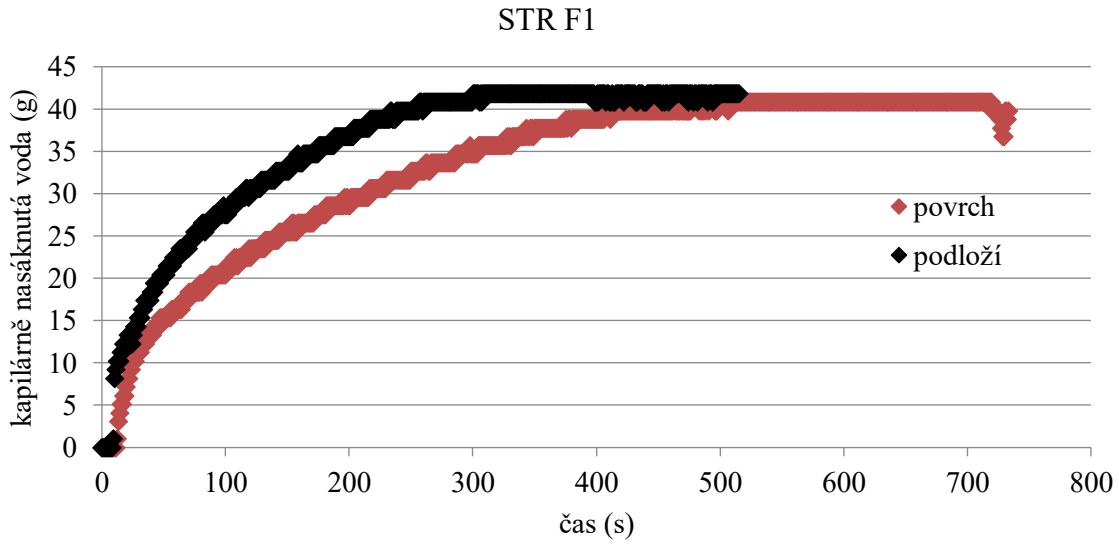

Obr. P2.11. Měření rychlosti kapilárního nasákávání pro vzorek ze sublokality STR F1. Na této lokalitě není přítomná biogenní skalní kůra; jsou uvedena měření skrz podloží a skrz povrch bez biogenní skalní kůry.

2.3. Grafy měření rychlosti kapilárního nasákávání v terénu

Na obrázcích obr. P2.12 až obr. P2.17 jsou uvedeny grafy znázorňující průběh měření rychlosti kapilárního nasákávání v terénu pomocí Karsten tube. Měření pro lokality ML1, ML2 a STR.

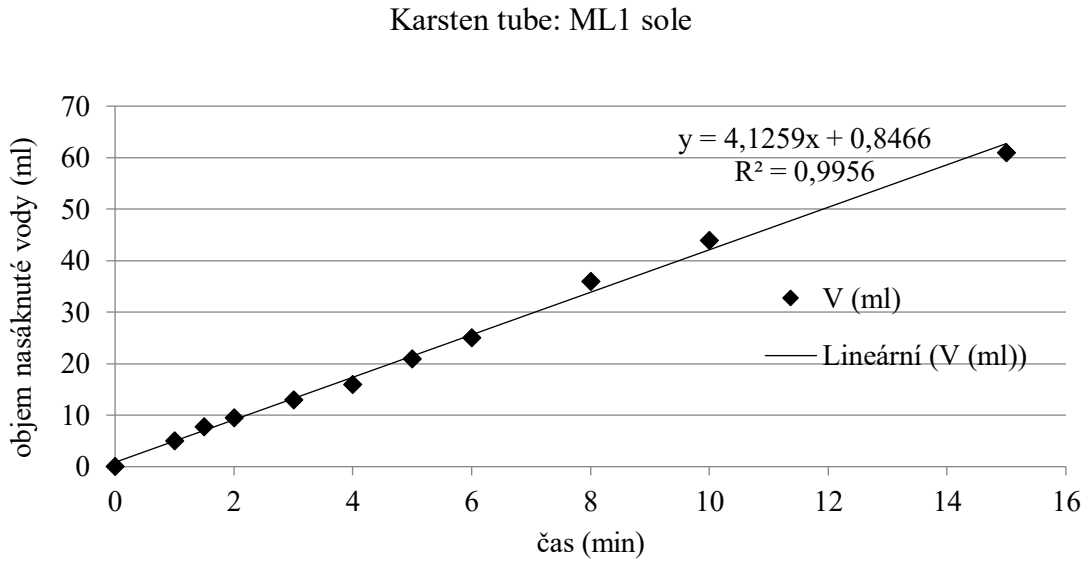

Obr. P2.12. Měření rychlosti kapilárního nasákávání v terénu pomocí Karsten tube na sublokalitě ML1 sole (měření skrz povrch).

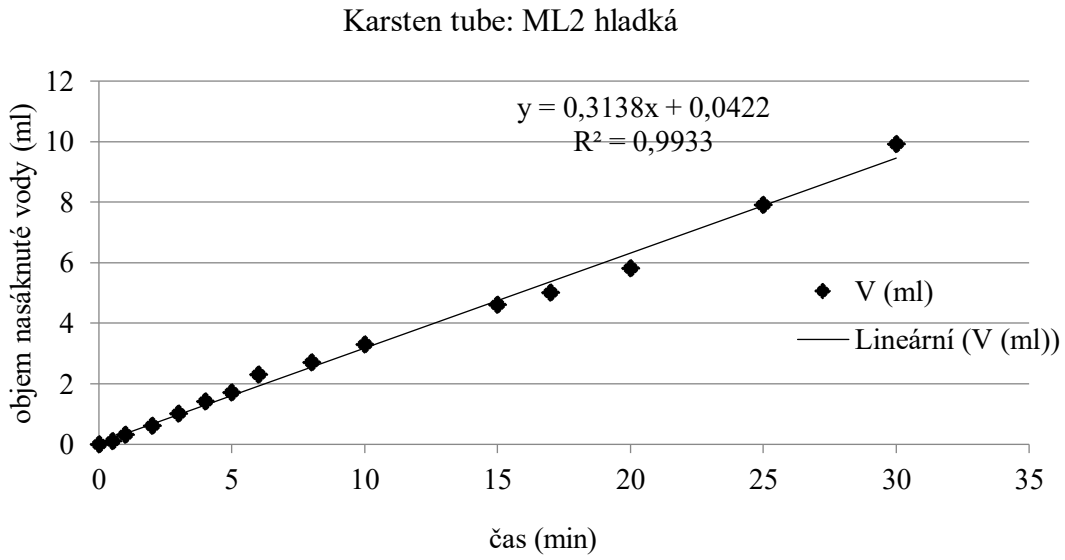

Obr. P2.13. Měření rychlosti kapilárního nasákávání v terénu pomocí Karsten tube na sublokalitě ML2 hladká (měření skrz povrch).

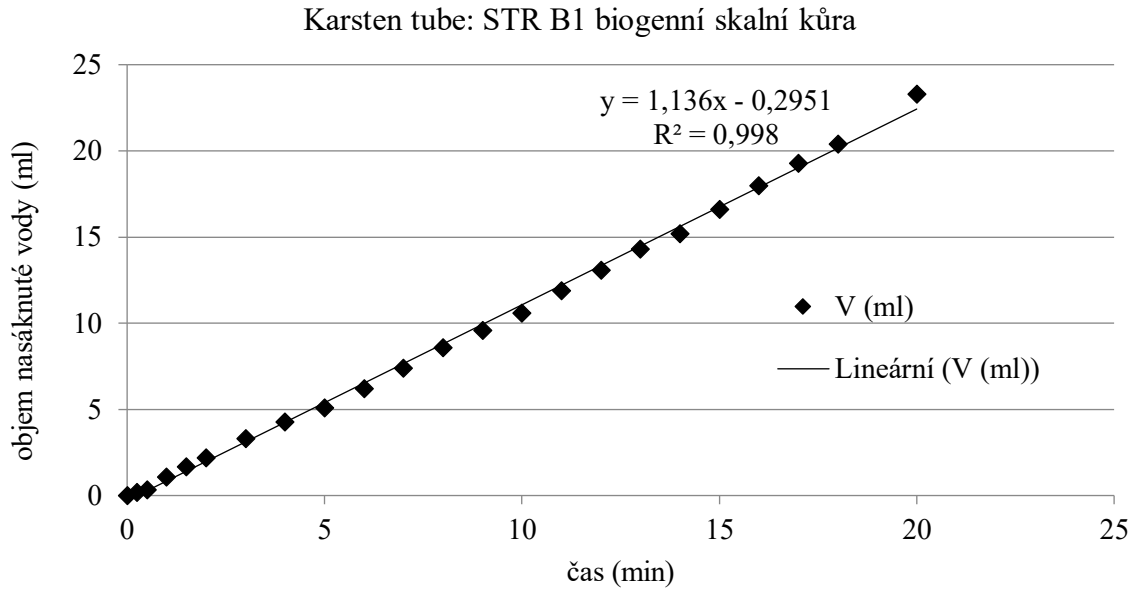

Obr. P2.14. Měření rychlosti kapilárního nasákávání v terénu pomocí Karsten tube na sublokalitě STR B1 (měření skrz povrch s biogenní skalní kůrou).

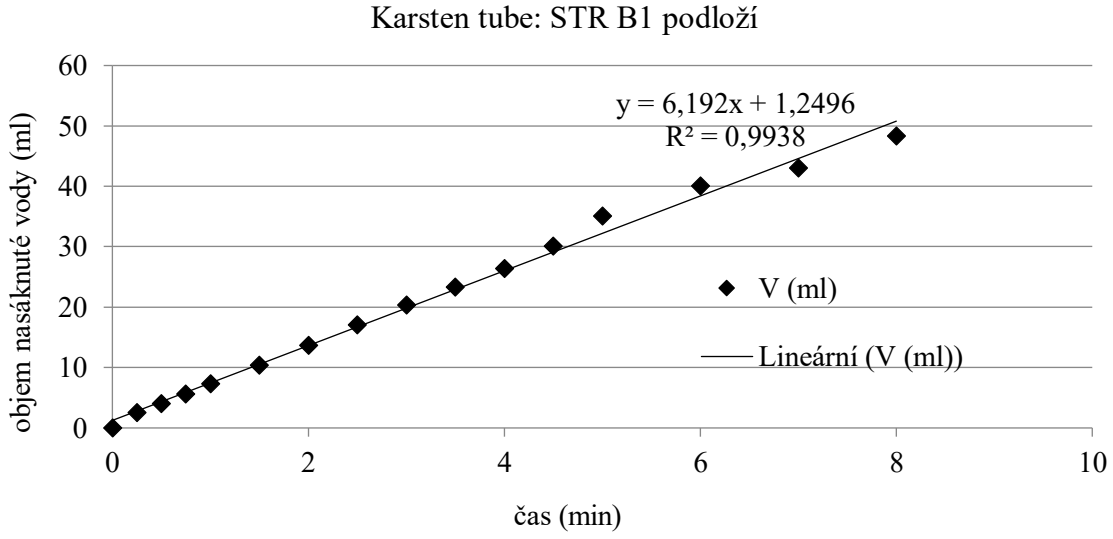

Obr. P2.15. Měření rychlosti kapilárního nasákávání v terénu pomocí Karsten tube na sublokalitě STR B1 (měření skrz podloží bez biogenní skalní kůry). Měření v tomto případě trvalo pouze 8 minut, neboť poté došlo kvůli podmáčení k odlepení ústí Karsten tube od pískovce.

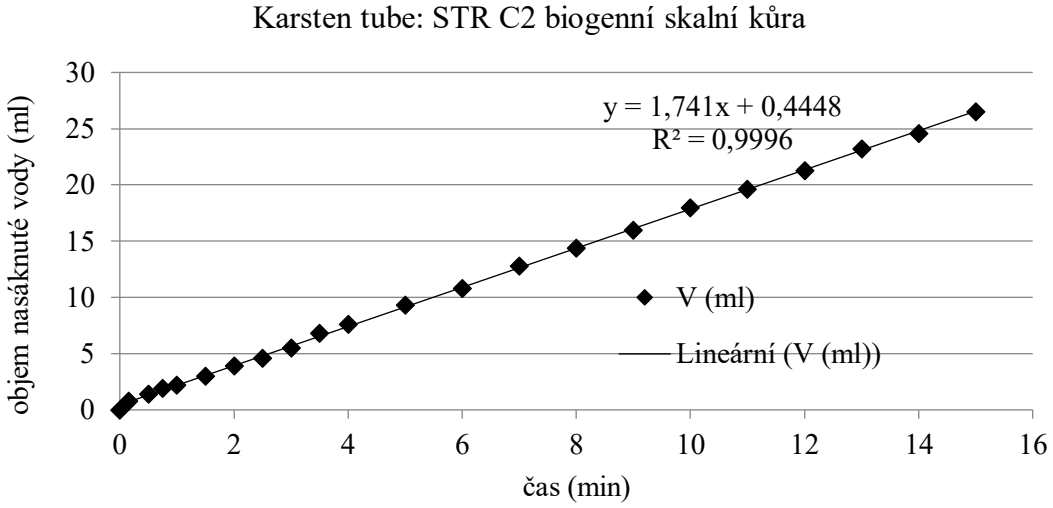

Obr. P2.16. Měření rychlosti kapilárního nasákávání v terénu pomocí Karsten tube na sublokalitě STR C2 (měření skrz povrch s biogenní skalní kůrou).

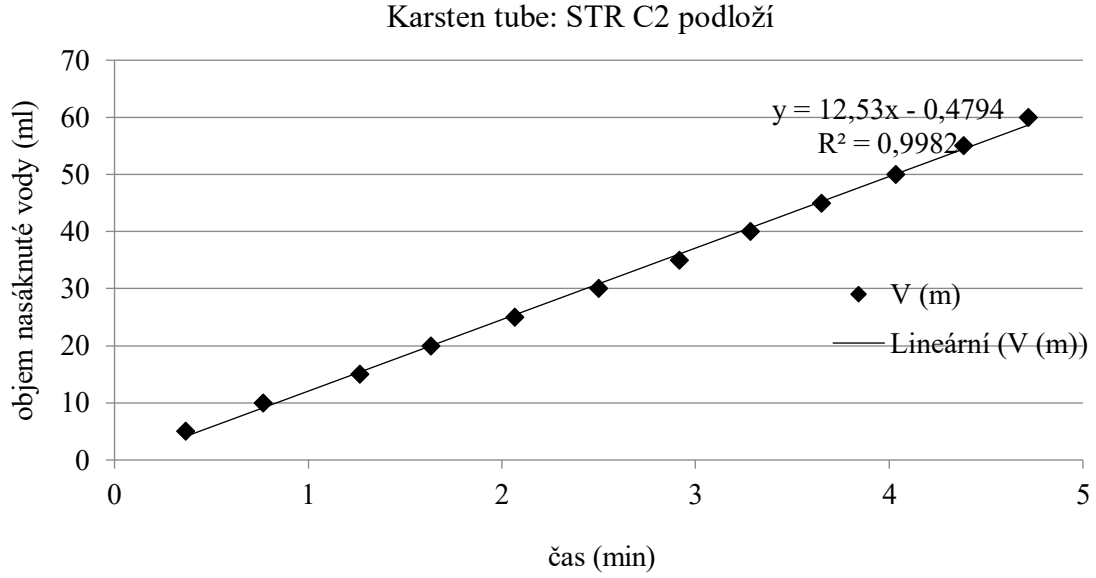

Obr. P2.17. Měření rychlosti kapilárního nasákávání v terénu pomocí Karsten tube na sublokalitě STR C2 (měření skrz podloží).

3. PŘÍLOHA 3

Publikace

Slavík, M., Bruthans, J., Filippi, M., Schweigstillová, J., Falteisek, L., Řihošek, J. (2017). Biologically-initiated rock crust on sandstone: Mechanical and hydraulic properties and resistance to erosion. Geomorphology 278, 298–313.

Geomorphology 278 (2017) 298–313

Contents lists available at ScienceDirect

Geomorphology

journal homepage: www.elsevier.com/locate/geomorph

Biologically-initiated rock crust on sandstone: Mechanical and hydraulic properties and resistance to erosion

Martin Slavík [a], Jiří Bruthans [a,*], Michal Filippi [b], Jana Schweigstillová [c], Lukáš Falteisek [a], Jaroslav Řihošek [a]

[a] Faculty of Science, Charles University, Albertov 6, 128 43 Prague 2, Czech Republic
[b] Institute of Geology, CAS, v.v.i., Rozvojová 269, 165 00 Prague 6, Czech Republic
[c] Institute of Rock Structure and Mechanics, CAS, v.v.i., V Holešovičkách 41, 182 09 Prague 8, Czech Republic

ARTICLE INFO

Article history:
Received 18 May 2016
Received in revised form 29 September 2016
Accepted 29 September 2016
Available online 23 November 2016

Keywords:
Biofilm
Biocrust
Biologically-initiated rock crust
Sandstone protection
Case hardening

ABSTRACT

Biocolonization on sandstone surfaces is known to play an important role in rock disintegration, yet it sometimes also aids in the protection of the underlying materials from rapid erosion. There have been few studies comparing the mechanical and/or hydraulic properties of the BIRC (Biologically-Initiated Rock Crust) with its subsurface. As a result, the overall effects of the BIRC are not yet well understood. The objective of the present study was to briefly characterize the BIRC from both the mineralogical and biological points of view, and especially to quantify the effect of the BIRC upon the mechanical and hydraulic properties of friable sandstone. The mineralogical investigation of a well-developed BIRC showed that its surface is enriched in kaolinite and clay- to silt-sized quartz particles. Total organic carbon increases with the age of the BIRC. Based on DNA sequencing and microscopy, the BIRC is formed by various fungi, including components of lichens and green algae. Using the method of drilling resistance, by measuring tensile strength, and based on water jet testing, it was determined that a BIRC is up to 12 times less erodible and has 3–35 times higher tensile strength than the subsurface friable sandstone. Saturated hydraulic conductivity of the studied BIRC is 15–300 times lower than the subsurface, and was measured to also decrease in capillary water absorption (2–33 times). Water-vapor diffusion is not significantly influenced by the presence of the BIRC. The BIRC thus forms a hardened surface which protects the underlying material from rain and flowing water erosion, and considerably modifies the sandstone's hydraulic properties. Exposing the material to calcination (550 °C), and experiments with the enzyme zymolyase indicated that a major contribution to the surface hardening is provided by organic matter. In firmer sandstones, the BIRC may still considerably decrease the rate of weathering, as it is capable of providing cohesion to strongly weathered (and disintegrated) sandstone surfaces. However, only a near-surface zone of the sandstone is stabilized by the BIRC, and additional sources of stabilization (gravity-induced stress, inorganic cement, etc.) contribute to the resistance of the subsurface zone of sandstone exposures.

1. Introduction

Due to its complexity and contact with the atmosphere, a sandstone surface is a critical zone, with properties affecting the erosion rate. Along with abiotic weathering and erosion factors, biotic factors are considered to play an important role both in the deterioration and stabilization of sandstone surfaces (Gorbushina, 2007 and references therein). Biocolonization on sandstone surfaces is known to play an important role in rock disintegration, yet it sometimes also aids in the protection of the underlying materials from rapid erosion. Our study is concerned with the effect of biologically-initiated rock crust on the mechanical and hydraulic properties of friable sandstone and its resistance to erosion.

1.1. Biocolonization of sandstone surfaces

Various types of organisms and their communities can be found on rock surfaces (epilithic) as well as within their subsurface (endolithic) (Goloubic et al., 1981; Hirsch et al., 1995; Hallmann et al., 2013).

Different terms are used for these organisms and/or for the whole biologically-affected surface zone of sandstone, based on the range of the biological impacts, species, kinds of growth, or other characteristics; and are also based on the scientific field. The most common terms biofilm,

Abbreviations: BSE, backscattered electrons; BIRC, biologically-initiated rock crust; B-surface, uneven non-tectonic surface with a developed BIRC; C-surface, exposed surface of a tectonic fracture with a developed BIRC; EPS, extracellular polymeric substances; F-surface, surface of tectonic fracture without a BIRC; K, hydraulic conductivity; PBS, phosphate buffered saline; REI, relative erodibility indicator; SEM, scanning electron microscope; TOC, total organic carbon; TS, tensile strength; TSP, tensile strength parallel with the surface; TSP_{dry}, tensile strength parallel with the surface done on dried prisms; TSP_{wet}, tensile strength parallel with the surface done on wet prisms; Tx, capillary water absorption rate; δ, diffusion coefficient.

* Corresponding author.
E-mail address: bruthans@natur.cuni.cz (J. Bruthans).

http://dx.doi.org/10.1016/j.geomorph.2016.09.040
0169-555X/

bio-coating, biotic crust, biocrust, or simply crust are used for the complex communities of organisms living on the rock surface and/or penetrating it to depth (for references and details see Supplementary material). This paper deals specifically with the young biologically-inhabited and hardened sandstone surface and near subsurface zone of the rock including both the epilithic and endolithic microorganisms. Therefore, in this paper we used the term "biologically-initiated rock crust" – BIRC.

In general, the biologically-affected surface zone of sandstone reaches to several millimeters in depth (Gómez-Alarcón et al., 1995; Chen et al., 2000; Lisci et al., 2003). Due to their modular and adaptable growth, fungi dominate in the BIRC, and fungal hyphae may constitute >90% of the biomass volume (Bjelland and Thorseth, 2002; Gorbushina, 2007). Other common organisms are cyanobacteria, algae and bacteria (Ahmadjian, 1993; Hirsch et al., 1995). Development of microcolonies embedded in extracellular polymeric substances (EPS) is responsible for binding cells and other particulate matter together and to the substratum (Warscheid and Braams, 2000). A moist, sticky surface provided by the EPS may promote the trapping of airborne clay (Dade et al., 1990).

1.2. Role of microorganisms in erosion and protection

A great number of studies have been focused on the effects of microorganisms on rock surfaces (Gorbushina, 2007). Several studies demonstrated clear evidence of biodeterioration/bioweathering (e.g., Friedmann, 1982; Paradise, 1997; Robinson and Williams, 2000). Mechanical damage mainly proceeds due to penetration of the substrate by hyphae, as well as the expansion and contraction of lichen thalli due to changes in moisture content (Wessels et al., 1995; Lisci et al., 2003). Biochemical weathering is mediated by both organic and inorganic acids as well as metal-complexing compounds (Bjelland and Thorseth, 2002). Fungi were found to play a considerable role in stone weathering, either as part of the lichen mycobiont (Smits et al., 2009; Cutler et al., 2013) or as free-living form (Chen et al., 2000). Cyanobacteria are clearly capable of dissolving quartz due to an increase in pH to 11 in the vicinity of photosynthesizing cells (Büdel et al., 2004; Brehm et al., 2005). Conversely, other studies have reported that the BIRC-related phenomenon is also capable of protecting sandstone surfaces from wind abrasion, raindrop impact, water flow, temperature variations, and deposition of salts; therefore, it can possibly decrease the erosion rate (Gómez-Alarcón et al., 1995; Grondona et al., 1997; Souza-Egipsy et al., 2004; Viles and Goudie, 2004). The protective role of a biotic crust is widely documented on soils in arid and semiarid landscapes, where they stabilize various friable surfaces, and also positively influence the hydrology and other parameters (e.g., Warren, 1995; Kidron, 1999; Langhans et al., 2009; Pointing and Belnap, 2012).

Among other parameters, the moisture content, saturated hydraulic conductivity (K), vapor permeability, and capillary water absorption were measured to characterize the decrease of permeability of the pore space caused by the presence of BIRC (cf., Dennis and Turner, 1998; Thullner et al., 2002; Seifert and Engesgaard, 2012). It is important input data as water transport and moisture affect many weathering processes (Mol and Viles, 2013; Paradise, 2002). It was found that the BIRC modifies the capillary water uptake, causing measurable alterations in water-vapor diffusion, and surface-active compounds of biotic origin protect the microorganisms against water loss and desiccation (Warscheid and Braams, 2000).

The protecting effect of BIRC is commonly inferred from comparisons of lichen-inhabited and lichen-free surfaces (e.g., Arino et al., 1995; Mikuláš, 1999). However, most of above-mentioned studies neglect the possibility that biota may, in fact, already colonize relatively stable surfaces, and thus their presence might be the consequence, not the cause of the surface stability. Only a few studies have directly proven the stabilizing effect of the biotic crust (Kurtz and Netoff, 2001).

To our knowledge, there have been no studies published dealing with the quantification of both the mechanical and hydraulic properties (i.e., the parameters critical for weathering) of BIRC sandstone surfaces and their deeper subsurface zone. We believe that such information may disclose the role of biocolonization (i.e., formation of the BIRC) in the erosional response of weak sandstone exposures.

1.3. Objectives

The major objective of this study was to determine how the BIRC changes the mechanical and hydraulic properties of a weak sandstone surface, and how it influences resistance to erosion. The following partial tasks were resolved in order to fulfill this objective:

1) A brief characterization of the BIRC from both the mineralogical and biological points of view to determine whether the mechanical properties of BIRC are caused by organic or inorganic matter.
2) Determination and evaluation of the properties measured on the BIRC, in the deeper subsurface below the BIRC (i.e., in the original sandstone), and also on the bare surface.
3) A comparison of the properties of the initial and matured BIRC in order to elucidate the rate of colonization and hardening of the sandstone surface.
4) Determination if the BIRC is sufficient to protect the sandstone surface or if other factors are involved in the hardening of young weak sandstone surfaces.

In addition, we examined the effect of gravity-induced stress (i.e., internal rock pressure caused by gravity loading) onto a studied sandstone surface, since it has recently been found that increased gravity-induced stress strongly decreases the weathering and erosion rate of friable sandstone (Bruthans et al., 2014).

To achieve the above listed tasks, the study was focused on the BIRC and bare surfaces of a friable sandstone in a quarry, which had several benefits: (i) the surfaces are young (years to decades), so the effect of long lasting processes (like mineral case hardening) is unlikely; (ii) the contrast in properties of the BIRC and the deeper subsurface zone (i.e., inner friable and permeable sandstone) could be significant; and (iii) commonly used destructive techniques could be applied here.

2. Study site and sandstone characterization

The study area was the active Střeleč Quarry situated close to the Bohemian Paradise Protected Landscape Area in the Czech Republic (Fig. 1; Bruthans et al., 2012). The whole area is formed by the Hrubá Skála Sandstone formation and it is known due to attractive "rock cities" with numerous pinnacles up to 60 m high, as well as overhangs, arches and other landforms (Adamovič et al., 2006). Mean annual precipitation in the area is 790 mm (Holenice 2005–2014, Czech Hydrometeorological Institute).

Fine to medium grained quartz sandstone, with a planar stratification (4–18° to south-southwest), is interpreted as a coarse-grained delta body deposited in a shallow marine environment during the Turonian, Cretaceous (Uličný, 2001).

The study was focused on the so-called glass industry sandstone, which is white if freshly exposed on quarry faces, and yellowish to light green/gray if covered by a BIRC. Its matrix consists of kaolinite, quartz silt, and minor illite. Kaolinite is the primary cementing agent for the quartz grains, although contact diagenetic silica cement has developed locally (Hauser et al., 1965). The mean sandstone density is 2.0 g/cm^3, the porosity is 22%, the clay fraction content is 1.4%, and K is 5.10^{-5} m/s.

The sandstone studied is more friable than common cemented sandstones in the Bohemian Cretaceous Basin; the firmest portions of the sandstone have a mean uniaxial compressive strength of 14 MPa and a tensile strength of 280 kPa (Bruthans et al., 2012). On the other hand, some zones of the sandstone in the quarry are

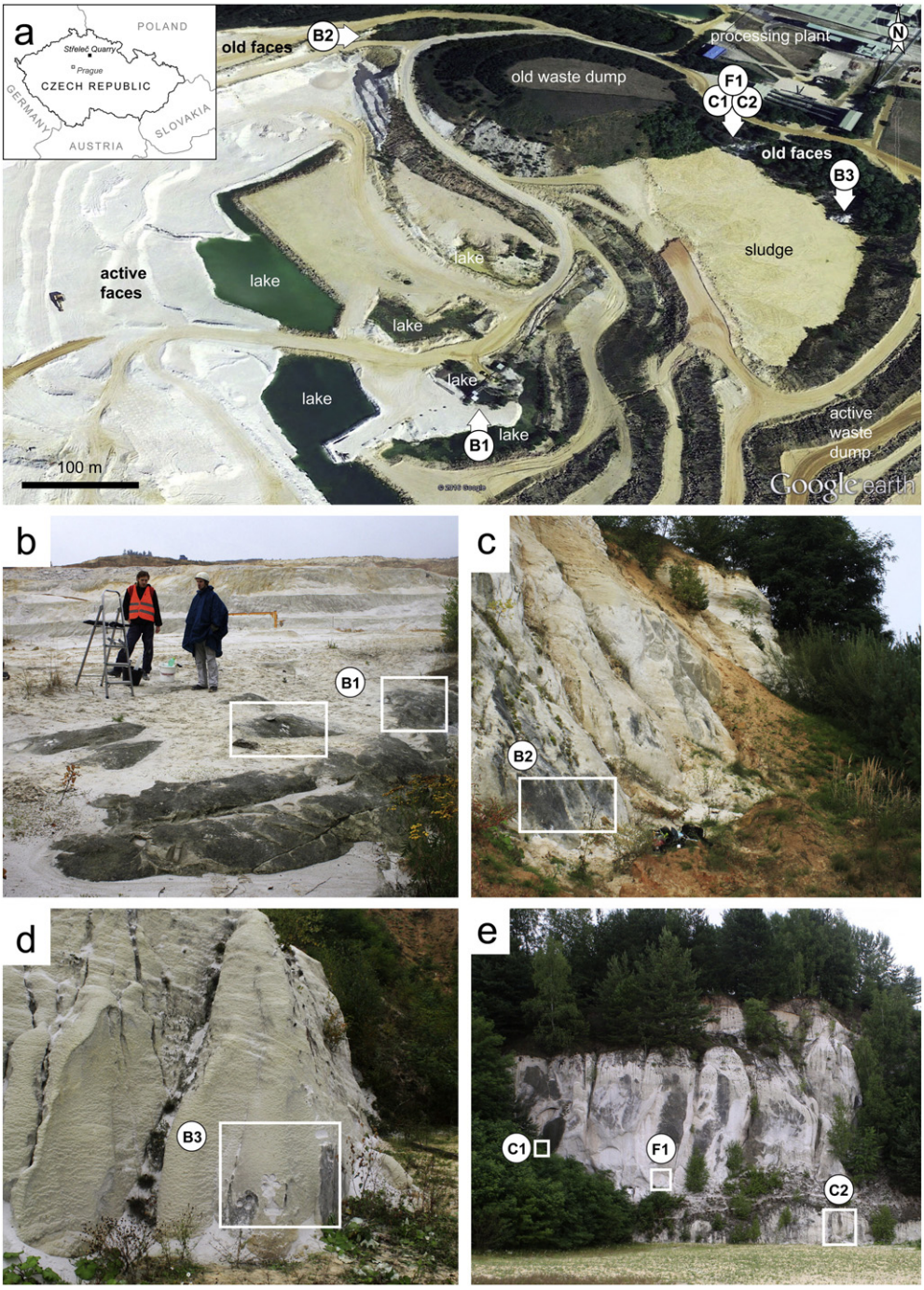

Fig. 1. Study area - Střeleč Quarry in the Czech Republic (source Google Earth): a) Positions of the different studied sites within the quarry; b) Non-tectonic surface of an abandoned quarry face with BIRC (B-surfaces) at the B1 (b), B2 (c), and B3 (d) sites; e) Abandoned quarry face representing surfaces of tectonic fractures with BIRC (C-surfaces) studied at the C1 and C2 sites, and surface of tectonic fracture without a BIRC (F-surface) studied at the F1 site. Rectangles on the photos represent the main sampling areas. For site characteristics see Section 2.0 and Table 1.

cohesionless and the material is called locked sand (Bruthans et al., 2014). Locked sand is only cemented by kaolinite. Its uniaxial compressive strength is 3 MPa due to the interpenetrative fabric of the quartz grains. The tensile strength of locked sand is 2–4 orders of magnitude lower than the compressive strength, depending on moisture content as well as gravity-induced stress, due to the lack of mineral cement (Bruthans et al., 2014). Gravity-induced stress is capable of protecting the locked sand from erosion by rain and flowing water. Similarly, the cemented portions of the Hrubá Skála Sandstone show a considerable decrease in frost and salt weathering rate if subjected to gravity-induced stress (Bruthans et al., 2014).

Three different types of surfaces were selected for the study to distinguish the simple effects of the BIRC from the effects of tectonic fractures, which often display markedly lower erodibility than the other types of surfaces in the quarry (Bruthans et al., 2012):

(i) an uneven non-tectonic surface of abandoned quarry faces with a developed BIRC was called a B-surface (derived from "BIRC surface");

(ii) an exposed surface of a tectonic fracture with a developed BIRC was called a C-surface ("combined surface");

and (iii) a surface of tectonic fracture without a BIRC was called an F-surface ("fracture surface"; Fig. S1 in supplementary material).

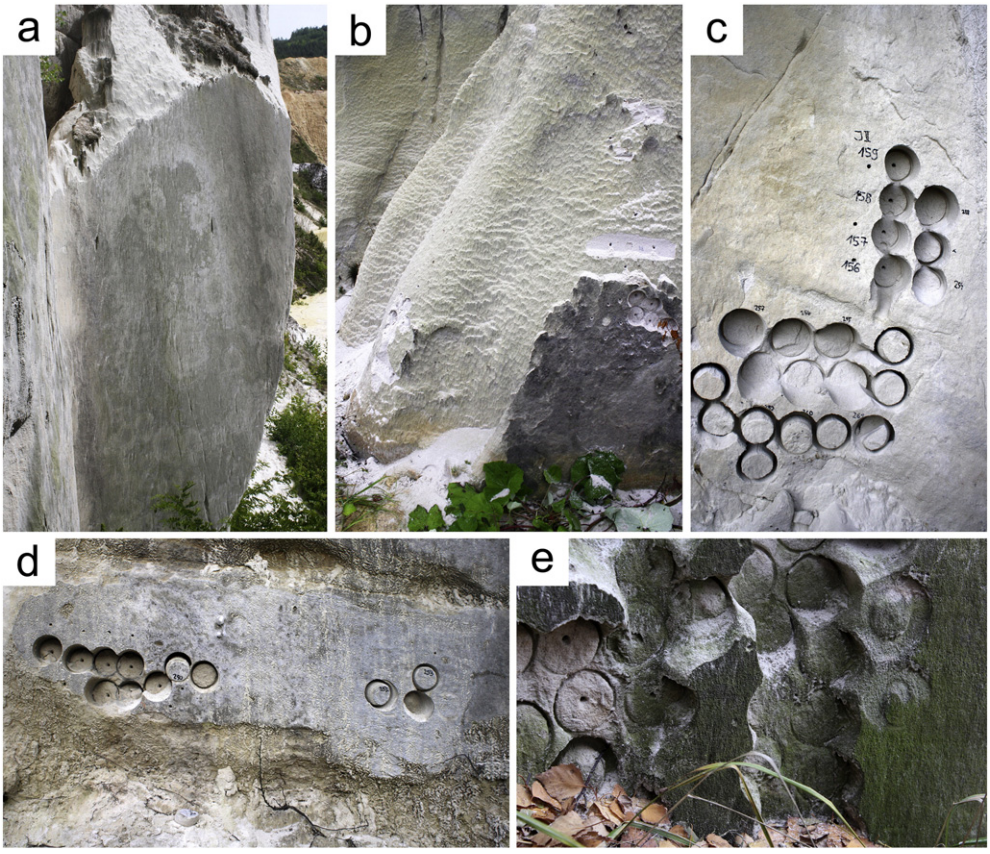

Fig. 2. Detailed views on some study sites: a) Exposed flat surface with BIRC from above, partly destroyed by erosion (C1 site); b) Eroded (freshly exposed) surface (white sandstone) with a relic of the BIRC (dark sandstone) at the B3 site; c) Positions of some drilled cores at the F1 site; d) Positions of some drilled cores at the C2 site; e) BIRC of various ages - successive sampling at the C1 site.

Six sites (B1, B2, B3, C1, C2, F1) were studied in the quarry (Figs. 1, 2; Table 1). The sites are exposed to insolation; only the C1 site was partly shaded by small trees. In the remainder of the text, those cores having a surface zone are called outer cores, while those cores solely composed of underlying material are called inner cores (Fig. 3). Besides the original BIRC (10–50 years old), a new BIRC which formed in two years on the cored surface was studied at sites B1, B2, and C1.

3. Methods

In this study we combined various methods and approaches, some of which are unconventional for sandstone research. Therefore, the methods are clustered here into relative groups and details for the particular procedures are presented as supplementary material.

Data obtained from the measurements were statistically tested using Student's *t*-test with significance level of $p \leq 0.05$.

3.1. Sampling and sample treatment

For sampling, an accumulator hand drilling machine with a diamond crown core drill (67 and 83 mm in diameter) was used in a rotational mode, without percussion and without the use of water as a coolant. The lengths of drilled cores were 20–60 mm. All cores were tightly wrapped in foil in the field to prevent the material's failure during transport and other treatments. In the laboratory, the foil was gently removed except for some of the mechanical measurements (see below). If not otherwise stated, the cores were dried under laboratory conditions (20 °C; ~50% relative humidity) until reaching a stable weight. Standardized dried cores were used for all tests except where stated differently. In addition, tensile strength measurements (see below) were also done with partly re-saturated materials (suction pressure ~1 kPa). Mechanical tests were also done with calcined cores (i.e., cores heated to 550 °C for 20 h in an electric furnace to incinerate organic matter). Other details concerning the core cylinder treatments are stated in the Supplementary material.

Table 1
List of study sites in the Střeleč Quarry.

Site	Surface type	Aspect	Surface inclination	Surface age (y)	Volumetric moisture content (%)	Open to rain
B1	B surface	NW	5–20°	10	3.7–7.2	Yes
B2	B surface	SW	50°	13	3.4–4.6	Yes
B3	B surface	W-SW	70–80° (in overhang)	<50	5.2–6.6	Yes
C1	C surface	NW	80°	~50	0.8–3.0	Yes
C2	C surface	W	90°	~50	3.0–3.4	Partly
F1	F surface	NW	80°	~50	0.1–1.2	No

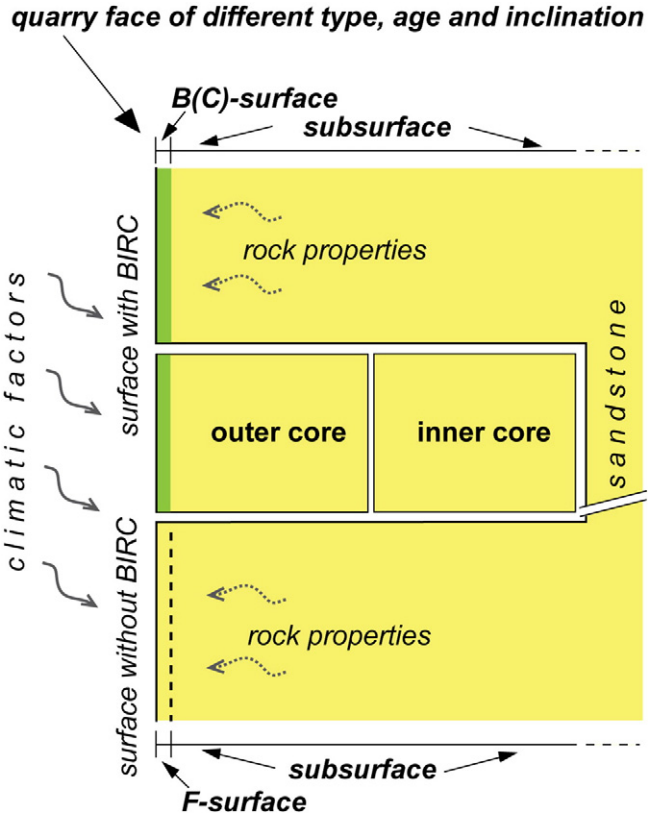

Fig. 3. Drawing explaining the terminology related to the sampling - i.e., type of sandstone surfaces studied, positions of drilled cores, and definition of the surface and subsurface samples. Precipitation impact, sun radiation, frost, and wind action, etc. represent the outer factors affecting the rock exposures; while moisture, porosity, content of clay particles, etc. represent the inner factors.

As sample treatment for the hydraulic properties measurements was complicated, some cores were used both for measuring K and water vapor permeability. In the case of mechanical properties, a separate core was used for each method.

3.2. Sample characterization

3.2.1. Microscopic methods

The microscopic study of hand specimens was performed using an OLYMPUS SZX16 binocular stereo microscope with a digital photo camera and photos were processed by a QuickPHOTO Micro software and a Deep module. A QUANTA 450 (FEI, USA) scanning electron microscope (SEM), equipped with an energy dispersive spectrometer system (Apollo X, EDAX, USA) and a photomultiplier detector for backscattered electrons (BSE) was used for sample characterization. The samples were cut in sections perpendicular to the surface, impregnated with epoxy, polished, and coated with gold or carbon. To study the penetration and amount of biological material within the sandstone, the same sections were polished again and stained with Pb-citrate (modified procedure according to Reynolds (1963)), washed, air dried, and re-coated with gold.

3.2.2. Total organic carbon and porosimetry

Total organic carbon (TOC) was determined as the difference between the content of total carbon and total inorganic carbon using an ELTRA CS 500 and 530 (ELTRA, Germany) simultaneous analyzers equipped with a resistance furnace (burning samples at 1350 °C). The detection limit was 0.1% for both methods. Prior to measuring, the BIRC was carefully separated from its subsurface. Since only small amount of the BIRC was sampled, all material taken was analyzed. At the sandstone surface, the TOC was expressed in g/m^2; the subsurface was expressed as g/m^3, as normalization to unit area was not possible.

The pore-size distribution was measured by high-pressure mercury porosimetry using an AutoPore IV 9520 instrument (Micromeritics, USA) and the skeletal (true) density, ρ_{He}, was determined by means of a gas pycnometer instrument. More details are presented in supplementary material.

3.2.3. Characterization of microorganisms and their role in material cohesion

The fungi were identified by sequencing the ITS1, 5,8S rDNA, as well as the ITS2 region. The polymerase chain reaction products, prepared following Martínková et al. (2010), were cloned and about 10 clones from each sample were re-amplified and sequenced. The sequences were deposited into GenBank under accession numbers KU687385 - KU687402. Algae were plated on agar with Bolds basal medium and identified after 7 days. The role of fungi in the surface hardening was examined by incubation in PBS with 20 U of zymolyase and 1% dithioerythritol for 10 days at 37 °C. Preservation of the crust was compared with a PBS-only sample. Other samples were incubated overnight in 6 M guanidine hydrochloride, and in acidified 5% $KMnO_4$ at 90 °C. For the detailed procedure, please see the supplementary material.

3.2.4. Moisture content

The moisture content was measured in the cores. As the studied sandstone is friable, drilling only took several seconds, so the core was not significantly heated, and the moisture content was not altered. Cores were weighted immediately in the field, and again after drying in the lab. Differences in weights divided by the dry weight of the sample were multiplied by the dry sandstone density to obtain the volumetric moisture content.

3.3. Mechanical properties and erodibility

Three methods testing the mechanical properties were used: (i) drilling resistance as a measure of resistance to abrasion, (ii) tensile

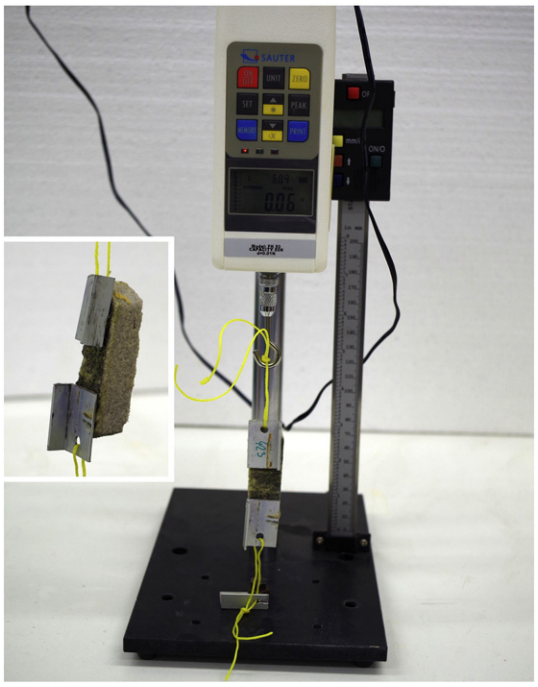

Fig. 4. Apparatus including a Sauter FH 50N tensiometer for measurement of tensile strength of surface and subsurface samples (prisms). Detail shows a prism prepared for measurement of the tensile strength parallel to the surface (TSP).

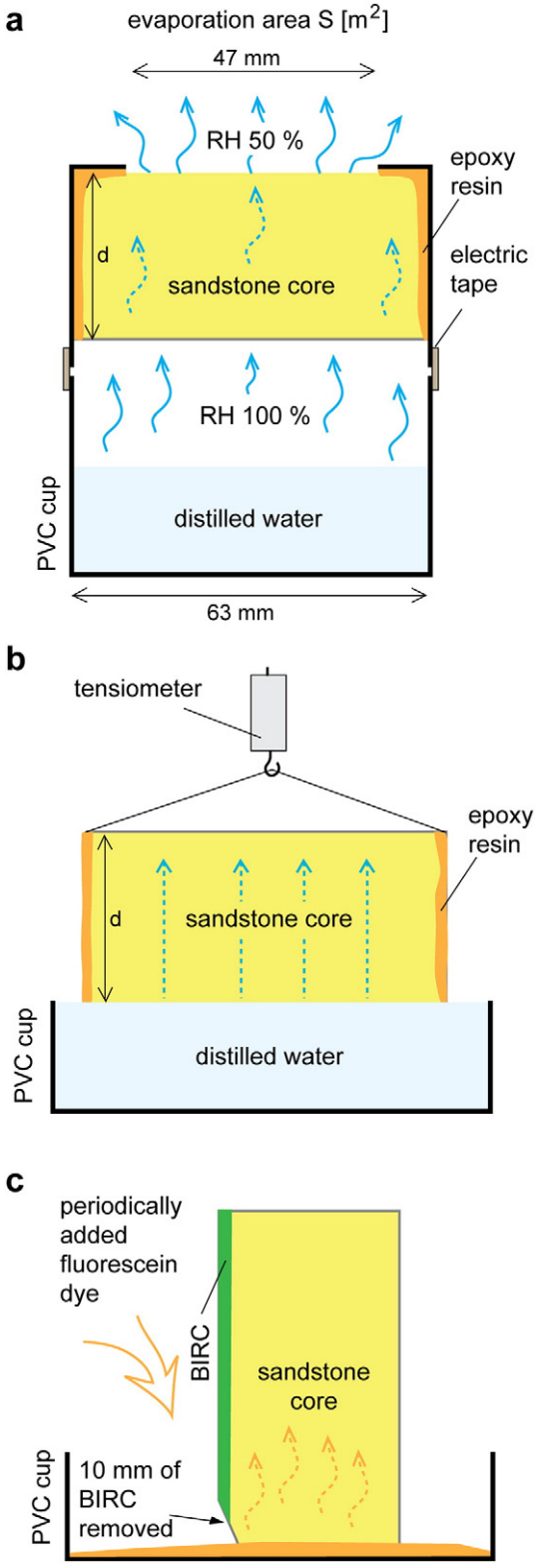

Fig. 5. Scheme of some hydraulic methods: a) Scheme of wet cups prepared for measuring water vapor permeability. PVC is abbreviation for polyvinyl chloride. Under the core, RH 100% was provided by distilled water, while 50% RH above the core was maintained by a CTC 256 Memmert climatic test chamber. Therefore, a humidity gradient was imposed in the core, and water vapor diffused upwards towards the area of lower partial vapor pressure; b) Scheme for measuring capillary water absorption. Core with cylinder sealed with epoxy resin was hung on a Sauter FH 50N tensiometer. The lower side of a core was in contact with the water surface, and the tensiometer recorded the increasing weight of the sample; c) Scheme of the fluorescein visualization of hydrophobicity in the cores (see Section 3.4.4).

strength as a measure of resistance to tensile stress, and (iii) a relative erodibility indicator that estimates the relative susceptibility to erosion.

3.3.1. Drilling resistance

Drilling resistance (i.e., drilling under controlled lab conditions expressed as the time needed to drill one millimeter) is a method commonly used to determine the sandstone subsurface properties such as the degree of weathering and influence of case hardening (Pamplona et al., 2007; Heinrichs, 2008; Siedel et al., 2010). A Tersis 2 drilling-machine (Geotron-Elektronik, Germany) was used with a 3 mm diameter

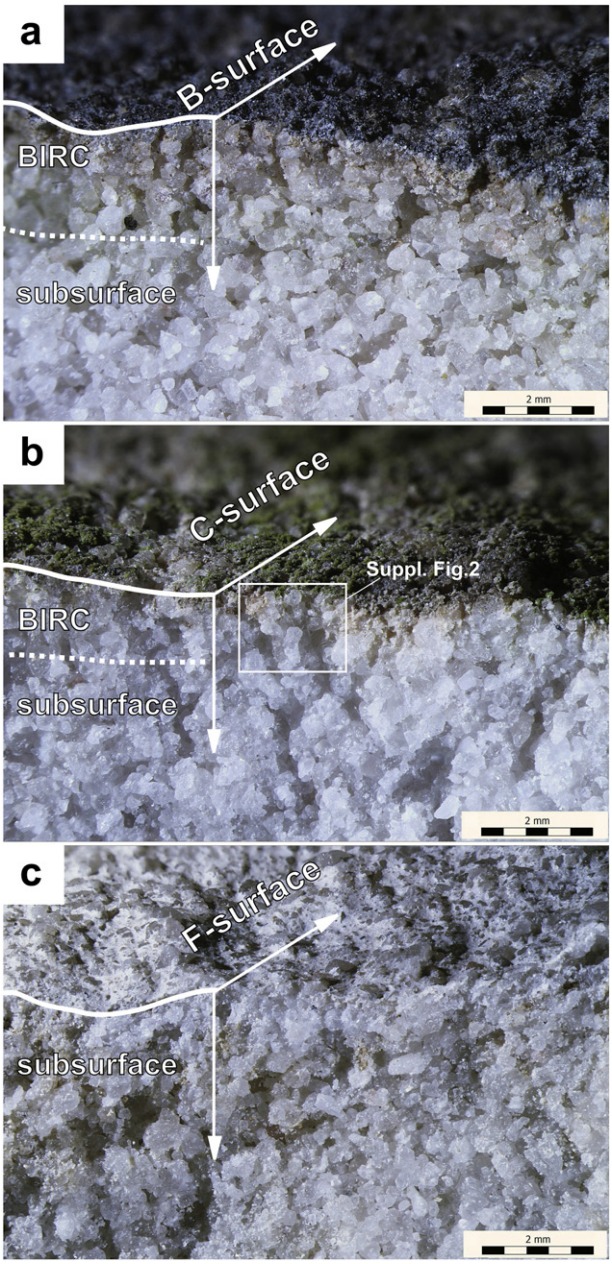

Fig. 6. Side view of the vertical sections of drilled cores showing the three different types of samples studied. Each photo shows surface and subsurface zone of the samples: a) B-surface from B2 site with mature BIRC with dark color caused by partly (temporarily) lifeless organic matter; b) C-surface from C1 site with well-developed fresh organic matter of green color. White rectangle shows position of a detail presented by Fig. S2 in the Supplementary material; c) F-surface from the F1 site lacking BIRC, but showing well recognizable kaolinite infilling among grains. For a better documentation of the surface of samples see Fig. S1 in the Supplementary material.

Table 2
BIRC thickness and relative drilling resistance (DR). Relative DR is the ratio of drilling resistance of the BIRC and subsurface. The average is given, with the range of values in parenthesis. Green zone thickness is based on macroscopic observations on polished sections. Fines SEM - thickness of zone enriched in fines.

Site	Crust thickness DR (mm)	Relative DR (surface/subsurface)	n	Green zone thickness (mm)	Fines SEM (mm)
B1	2.0–3.5	12 (2–51)	14	–	0.5–1.0
B2	2.0–3.0	5 (2–7)	3	3	0.5–1.5
B3	2.0–3.5	6 (2−11)	7	–	
C1	2.0–2.5	5 (2–9)	9	2.5–3	0.5–1.0
C2	2.0–6.0	4 (3–5)	6	3	0.5–2.0
F1	–	–	9	–	0.2–0.5

masonry drill bit. Constant pressure was used during individual drillings, depending on sandstone hardness (0.09–0.29 bar).

3.3.2. Tensile strength

In the field, the tensile strength (TS) was measured according to Bruthans et al. (2012, 2014) and calculated in kPa. The measurements were processed under the ambient moisture of the outcrop and after wetting the outcrop by intense watering for 30 min. Two types of surfaces were tested: the BIRC, and the subsurface zone reaching 2–6 cm below the BIRC.

Laboratory measurements of tensile strength were designed to compare the BIRC with the subsurface. To remove the effect of gravity-induced stress and interlocking of sand grains, the laboratory measurements were done on prisms (for details see Fig. 4 and the Supplementary material). The maximum force before failure divided by the area of the failure plane (kPa) is called the tensile strength parallel with the surface (TSP). As the tensile strength of the material is affected by moisture content (Bruthans et al., 2012), measurements were done under two different conditions: dried - TSP_{dry} (~50% relative humidity), and wet - TSP_{wet} (suction pressure ~1 kPa).

3.3.3. Erodibility

Relative susceptibility to erosion by flowing water and rain action (erodibility) was measured by means of a water jet according to the procedure used by Bruthans et al. (2012). The depth of the water jet drill hole was designated as the "relative erodibility indicator" (REI). The higher the REI value, the more erodible the material. As REI values measured in the field may be affected by inclination of the surface, measurements were performed on cores with the measured face oriented vertically. Measurements were done via both the surface and subsurface (three measurements for each side). To test the effects of organic matter on erodibility, some cores were calcined before measuring.

Evidence of erosion was sought at the sandstone surfaces at studied sites and in their vicinity. Material washed out from a small exposure of friable sandstone, lacking a BIRC, was collected over a one year period in the immediate vicinity of the B3 site (Fig. 1d). The erosion rate was calculated as the weight of the collected sand divided by the sandstone density, and the surface area from which the sand was washed out.

To test the stability of the sandstone and BIRC without a gravity-induced stress effect, the freshly drilled outer cores were exposed to rain erosion and frost weathering out in the open site. The cores were installed in varying positions: surface directed downward, upward, and with a steeply inclined surface. The erosion was periodically observed and photo-documented over a one year period.

3.4. Hydraulic properties

3.4.1. Saturated hydraulic conductivity (K)

K was measured in the cores under constant head flow conditions. To prevent the effect of air-bubbles on hydraulic conductivity, the samples were vacuum-saturated and the water used for the measurements was boiled and cooled just before measurements were taken. Two types of cores were used: outer cores and inner cores. K of the core given in m/s was calculated from Darcy's law and K of the BIRC itself was calculated according to the harmonic mean approach (Domenico and Schwartz, 1998; Supplementary material).

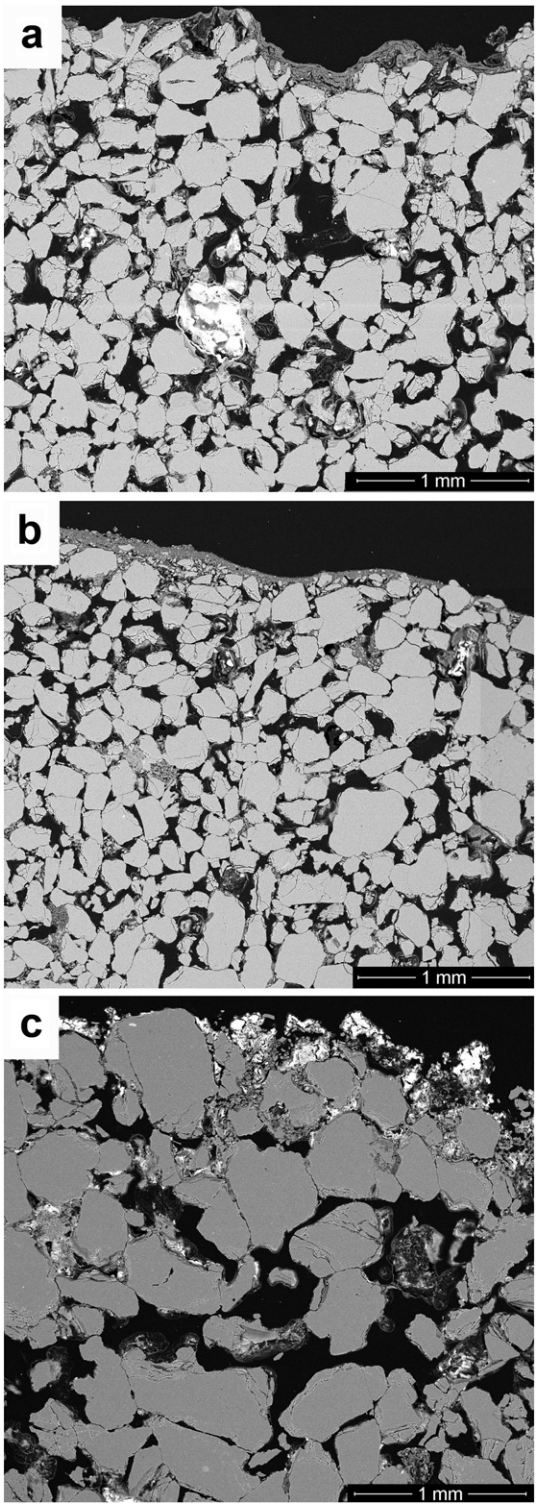

Fig. 7. BSE images of the polished sections (section perpendicular to the surface) through samples with a BIRC - C2 site (a) and without BIRC - F1 site (b). Images document similarity of sandstone under both surfaces – i.e., grain size, pore distribution, and especially enrichment by kaolinite on the surface (see darker coatings on the surface). Organic matter on the surface of sample (c) is not well recognizable by the BSE method and therefore it is highlighted (shining white) by staining with Pb-citrate (B2 site).

3.4.2. Vapor permeability

Water vapor permeability was determined according to the adapted norm "EN ISO 12572:2001". A similar experiment with sandstone was provided by Pavlík et al. (2008). Cores were placed into polyvinyl chloride cups with a 47 mm opening diameter, and were sealed with epoxy resin to prevent any escape of moisture. The outer cores were placed into the polyvinyl chloride cup with the surface zone facing upwards. Other polyvinyl chloride cups were partly filled with distilled water, which acted as a source of humidity (relative humidity 100%). Both were attached together and sealed with electrical sealing tape (Fig. 5a). This tape acts as an excellent sealant, two polyvinyl chloride cups sealed by tape transmitted <0.05 g of water in 24 days. Attention was paid to avoid any contact of the cores with the liquid water. Wet cups were placed into a CTC 256 Memmert climatic test chamber (Memmert, Germany) with a relative humidity of 50% and temperature of 20 °C, homogenized by fan. A humidity gradient was imposed in the core. The measurements lasted 21–28 days.

Due to the vapor-proof sealing, the water vapor diffusion via core can be approximated by 1D transport. The diffusion coefficient δ (s) and water vapor resistance factor μ were calculated based on equations in Pavlík et al. (2008; Supplementary material). Parameter μ shows how many times the studied sandstone was less permeable than still air of the same thickness. δ of the BIRC was calculated based on the harmonic mean approach.

3.4.3. Capillary water absorption

Water absorption to cores was measured using a Sauter FH 50N tensiometer (d = 0.01 N, capacity 50 N). The lower side of the core was put in contact with the water surface, and the weight of the sample was recorded at one second intervals until the maximum moisture content was reached by capillary intake (see also Fig. 5b). Decrease of the water level during measurement was negligible (<1 mm). Capillary water absorption was measured on each outer core in two directions: inflow via the surface and via the subsurface. For each direction, the capillary water absorption rate (Tx value in g m^{-2} s^{-1}) was determined by the equation presented in Supplementary material.

3.4.4. Visualization of hydrophobicity zones

To visualize the effect of the BIRC on capillary water transport, a sodium fluorescein dye was used at a concentration of 6.5 g/l, which is yellow, but a red color on evaporated places (Käss, 1998). Settings of the experiments are presented by Fig. 5c and also described in Supplementary material.

4. Results

4.1. Sandstone and BIRC characterization

Surfaces of samples with a BIRC are macroscopically green to dark gray, while samples without a BIRC are white (Figs. 6 and S1 in the Supplementary material). Based on SEM and optical microscopy the thickness of a BIRC reaches up to 2–3 mm (locally to 6 mm - see Section 4.2.1; Table 2). Optical and scanning electron microscopy of the polished sections showed that the surface zone (0.1–0.3 mm) is enriched in kaolinite and clay- to silt-sized quartz particles in most samples (Fig. 7a, b).

Table 3
Average values of total organic carbon (TOC) in the BIRC and subsurface.

Site	TOC in 10–50 years old surface [g/m^2]	TOC in ~2 years old surface [g/m^2]	TOC in young/old surface (%)	TOC in subsurface [g/m^3]
B1	44	6	14%	1.8
B2	40	9	23%	1.1
C1	155	16	10%	7.5
C2	8	–	–	0.7
F1	1	–	–	1.2

Table 4
Results of mercury porosimetry given as parameter ε.

Site	ε (porosity) surface	ε (porosity) subsurface	Surface pore size 10–100 μm (%)	Subsurface pore size 10–100 μm (%)
B1	0.27	0.31	77	84
B2	0.29	0.26	78	83
C1	0.23	0.28	73	88
C2	0.24	0.28	75	87
F1	0.35	0.40	80	90

Based on staining by Pb citrate, the organic matter is most abundant in the ~1–2 mm thick zone below the surface (Fig. 7c).

The BIRC is mainly formed by fungi and green algae (for details see Supplementary material). Based on the sequencing of 55 clones, 18 species-level clusters from phylogenetically and ecologically diverse lineages were determined. Only a small overlap in the composition of individual samples was observed, indicating that the fungi demonstrate both a great diversity and patchy distribution in the BIRC.

TOC content in the 10–50 year old BIRC varies between 8 and 155 g/m^2, while it is 4–10 times lower in ~2 year old BIRC (Table 3). Similar organic contents were found in the biologically initiated crusts on sandstones in South Africa and Antarctica (4–177 g/m^2; Friedmann, 1982; Büdel et al., 2004). In contrast, low TOC content at the F1 site (1 g/m^2) demonstrates well the absence of a BIRC.

Difference in porosity between subsurface and surface zone is 0.03–0.05 (Table 4). Most frequently, the pore size is 10–100 μm (73–80% of pores in the surface zone and 83–90% of the pores in the subsurface zone, including the F1 site). This indicates that decreased porosity of the surface is caused by fine inorganic particles (present also in F1 site) and not by the organisms forming the BIRC.

The calcined cores remained stable, and were also stable after flooding in water; except from B2 which had already been disintegrated after calcination. This shows that the sandstone, except at B2, has some permanent cement, probably quartz. On the contrary B2 is a locked sand (no permanent cement).

The measured data (Table 1) clearly shows that a BIRC only occurs on surfaces where the volumetric moisture content does not drop below a certain threshold (~1 vol.%). While site without a BIRC had a moisture content of 0.1–1.2 vol.%, sites with a BIRC had a moisture content of 0.8–7.2 vol.% This agrees with the study of Bellinzoni et al. (2013).

4.2. Mechanical properties and erodibility

4.2.1. Thickness of the BIRC and drilling resistance

The BIRC was detected on drilling resistance measurements as a hardened zone (Fig. 8). Based on the collected data, the thickness of the 10–50 year old BIRC varies between 2 and 3.5 mm, except at site C2 where it is 2–6 mm (Table 2). The two year old BIRC at the

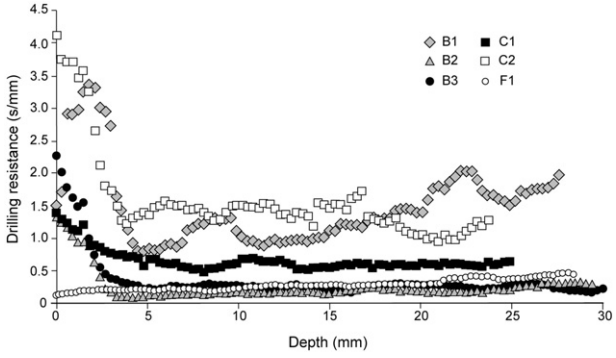

Fig. 8. Typical drilling resistance profiles for different sites. Depth below sandstone surface is on horizontal axis.

Table 5
Tensile strength parallel to the sandstone surface (TSP) measured in the laboratory. Average ± standard mean deviation is given, number of measurements is given in parentheses.

Site	Surface zone TSP_{dry} (kPa)	Subsurface TSP_{dry} (kPa)	Ratio TSP_{dry} surface/subsurface	Surface zone TSP_{wet} (kPa)	Subsurface TSP_{wet} (kPa)	Significant difference of TSP_{dry} between surface/subsurface?
B1	75 ± 18 (4)	26 ± 11 (2)	3	1.3 ± 0.3 (3)	0.8 (1)	S
B2	34 ± 6.5 (3)	<1.5	>22	3.4 ± 0.1 (2)	<1 (2)	S
C1	57 ± 38 (3)	6.7 ± 0.7 (3)	9	<1 (2)	0.9 ± 0.1 (2)	NS
C2	120 ± 0.7 (2)	3.4 ± 1.6 (2)	35	1.7 ± 0.6 (2)	–	S
F1	7.4 ± 3.9 (6)	4.5 ± 2.7 (3)	<1.6	1.6 (1)	1.3 ± 0.5 (2)	NS
C1 newly formed	16.4 ± 0.4 (2)	6.9 (1)	2	–	–	–

B1 site was only 2 mm thick. These findings accord well with the microscopic observations (see Section 4.1). However, the 2 year old BIRC at the C1 site was not yet detectable by drilling resistance, which indicates that surface hardening is slower than colonization by the BIRC. This might be caused by the slow accumulation of EPS and fungal hyphae. In general, the measured drilling resistance of the 10–50 year old BIRC is on average 4–12 times higher than the resistance of the subsurface (Table 2). On the other hand, no measurable differences between the surface and subsurface were found at the F1 site, with no observable BIRC. On the calcined B1 cores, the increased drilling resistance of the BIRC was no longer detectable. In the case of the calcined BIRC of the C2 site, BIRC drilling resistance was still two times greater than in the subsurface.

4.2.2. Tensile strength data interpretation

Values of tensile strength parallel to the sandstone surface (TSP) are listed in Table 5. For all sites except C1, the BIRC prisms had significantly higher dry tensile strength (TSP_{dry}) than subsurface ones by factor of 3–35 (Fig. 9a). The two year old BIRC also had an increased TSP_{dry} compared to its subsurface. On the contrary, no significant difference between the TSP_{dry} of the surface and subsurface was observed in the case of the F1 site without any BIRC.

TSP fails drastically when prisms are wetted (10–58 times compared to dry strength, Table 5). TSP_{wet} equals to a few kPa or less, both in the surface and subsurface prisms. This shows that the increased tensile strength of the BIRC is caused by the organic matter or clay, whose strength is compromised by moisture (Bruthans et al., 2014), and not

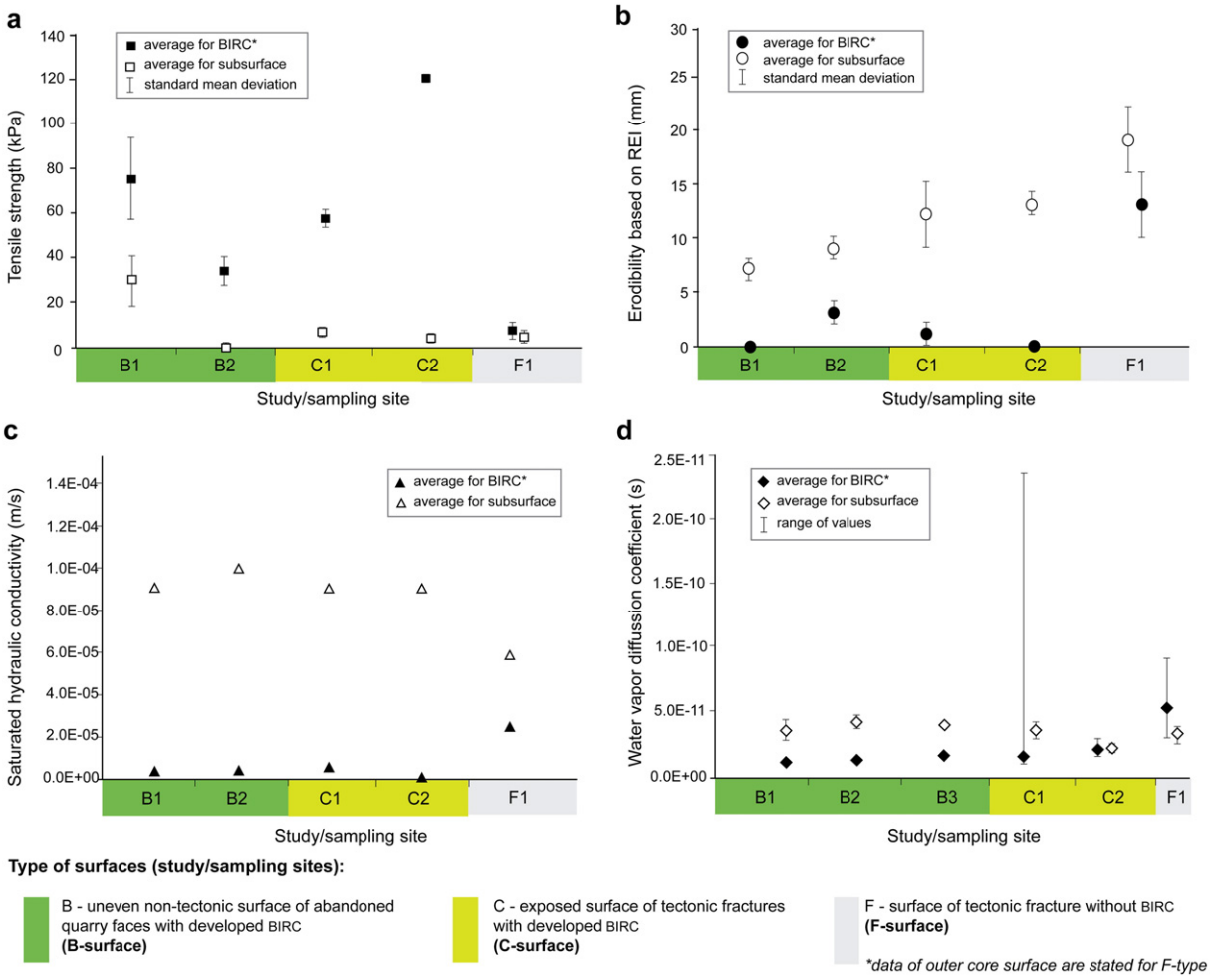

Fig. 9. Selected characteristics documenting different behaviors of samples with/without a BIRC: a) Tensile strength; b) Erodibility; c) Saturated hydraulic conductivity, and d) Water vapor diffusion.

Table 6
Tensile strength measured in situ (TS). Average is given, number of measurements is given in parentheses.

Site	Average TSa surface (kPa)	Average TSwet surface (kPa)	Ratio TSa/TSwet surface	Ratio TSa/TSP dry surface	Ratio TSwet/TSP wet surface	Average TSa subsurface (kPa)
B1	268 (5)	148 (6)	1.8	3.6	114	n.m.
B2	50 (3)	33 (4)	1.5	1.5	9.8	41
C1	245 (5)	121 (5)	2.0	4.3	>122	95

by silica cement, as the strength of covalently bonded quartz is not compromised by moisture.

TSP after calcination was only measured on the B1 samples, since the other samples were too friable. Calcination radically decreased the TSP_{dry}, and eliminated the difference between the TSP_{dry} and TSP_{wet}; demonstrating well that organic matter is the dominant source of the tensile strength in the BIRC.

Above mentioned measurements were done on small sandstone prisms with free sides.

As shown by Bruthans et al. (2014), the behaviors of free samples can differ greatly from the behavior of the same sandstone when locked within a massive rock outcrop due to the interlocking of sand grains and gravity-induced stress. To test if a drastic decrease of tensile strength after wetting will also occur in the field, we performed additional measurements on the sandstone outcrops. Unlike in the previous case, the tensile strength was measured in a direction perpendicular to the outcrop surface (TS), under ambient moisture and after wetting. The measurements are listed in Table 6. In the field the wet TS was just 1.2–2.6 times lower than the ambient TS, thus in distinct contrast with a drastic difference between the TSP_{dry} and TSP_{wet} in the lab. Interestingly, field ambient TS was 1.5 to 4 times higher than laboratory TSP_{dry} values, indicating some additional cohesion source in the field. The difference in the results between the laboratory and field measurements is discussed in detail in Section 5.3.

4.2.3. Erodibility

Jet tests showed a significant difference in erodibility between the surface and subsurface in the case of all sites with a BIRC (Fig. 9b, Table 7). While the REI of the BIRC was between 0 and 3 mm, the REI of its subsurface was 7–13 mm. Even the two year old BIRC showed significantly lower REI values than did the subsurface. However, the REI of two year old BIRC did not reach values measured in the 10–50 year old BIRC (Table 7). On the other hand, in the case of the F1 sample (with no BIRC), the surface erodibility was very high (13 ± 3 mm), and not significantly different from the subsurface. After removing the organic matter by calcination, the REI of the BIRC increased to 5–7 mm, but there was still a measurable difference between the surface and subsurface.

4.3. Hydraulic properties

4.3.1. Saturated hydraulic conductivity (K)

K of the inner cores is mostly 2–3 times higher than the K of the outer cores (Fig. 9c, Table 8). The largest difference is in the case of C2, where K of the inner core was 42 times higher than the outer core. To estimate K of the BIRC, K of the outer core was divided into two components (see Supplementary material): a thin BIRC with an unknown value of K, and a subsurface zone with K equal to the inner core (Eq. (3) in Supplementary material). BIRC thickness was derived from the drilling resistance (Table 2). The calculated K of the BIRC is 3×10^{-7} m/s in the case of C2, and $3–6 \times 10^{-6}$ m/s in the case of the other localities. K of the subsurface is between 6×10^{-5} and 1×10^{-4} m/s. The BIRC is thus ~300 times less permeable than its subsurface in the case of C2, and 15–35 times less permeable in the cases of the other sites.

As only a few samples were measured, and the Student *t*-test cannot be performed for each study site separately, data from all study sites were analyzed together. Following this approach, it was found that K of the BIRC is significantly reduced compared to its subsurface.

4.3.2. Water-vapor diffusion

The diffusion coefficient δ is $2–4 \times 10^{-11}$ s for the inner cores, and $2–5 \times 10^{-11}$ s for the B and C outer cores. The outer cores were 10–80% less permeable than the inner ones (Fig. 9d, Table 9). On the other hand, the F1 outer cores were 30% more permeable than the inner cores. To estimate the vapor permeability of the BIRC, the value of the diffusion coefficient of the outer core was divided into two components (see Supplementary material): a thin BIRC with an unknown value of the diffusion coefficient, and a subsurface zone with the diffusion coefficient equal to the inner core (Eq. (5) in Supplementary material). The mean diffusion coefficient of the BIRC is estimated roughly from 5×10^{-12} to 1×10^{-11} s for all sites. The higher permeability of the F1 outer cores shows that the F1 surface is several times more permeable than its subsurface; possibly due to surface weathering. The B and C BIRC is ~4–9 times and ~1–3 times less permeable to vapor diffusion than the subsurface, respectively. Vapor diffusion in the sandstone pore space of the subsurface was on average 4–9 times less effective than still air of the same thickness (μ value, Table 9).

However, due to the wide range of values, and due also to a lack of data (in the case of sites B2 and B3) (Table 9, Fig. 9), a significant difference in vapor diffusion between the BIRC and its subsurface was only found in one (B1) out of five study sites. When data from all the study sites were analyzed together, the BIRC was found to not significantly reduce water-vapor diffusion.

4.3.3. Capillary water absorption

The BIRC clearly alters the shape of the capillary absorption curve (Fig. 10). For all BIRC sites, the capillary absorption curve shape is convex if the capillary water enters the core via the BIRC, and concave if the capillary water enters the core via the subsurface (Fig. 10). A convex shape signifies a low initial permeability of the BIRC to capillary water, which steadily increases over time. A concave shape signifies a high initial permeability of the subsurface, followed by a decrease of the

Table 7
Mean and standard mean deviation of REI measurements. The slight differences between REI readings on the subsurface are caused by the variability of the sandstone. Site B3 was inaccessible at the time of sampling.

Site	10–50 years old surface (mm)	Subsurface (mm)	Surface ~2 years old (mm)	Subsurface (mm)	Calcinated surface (mm)	Calcinated subsurface (mm)	Significant difference of REI between surface/subsurface for BIRC 10–50 years old?
B1	0 ± 0	7 ± 1	2 ± 2 (1.9 yrs)	10 ± 3	5 ± 2	11 ± 3	S
B2	3 ± 1	9 ± 1	Not measured	–	Disintegrated	Disintegrated	S
C1	1 ± 1	12 ± 3	3 ± 1 (2.2 yrs)	8 ± 2	5 ± 0	9 ± 1	S
C2	0 ± 0	13 ± 1	Not measured	–	7 ± 1	8 ± 2	S
F1	13 ± 3	19 ± 3	Not measured	–	15 ± 4	12 ± 1	NS

Table 8
Measured saturated hydraulic conductivity (K) of inner and outer cores and calculated K of BIRC. Number of measurements is given in parentheses. K of B3 inner cores was not measured (n.m.) due to its friability.

Site	K outer c. (m/s)	K inner c. (m/s)	Ratio K inner/outer c.	K surface (m/s)	Ratio K subsurface/surface	Significant difference of K between surface/subsurface?
B1	3E−05 (1)	9E−05 (1)	2.9	3.8E−06	24	–
B2	4E−05 (1)	1E−04 (1)	3.2	3.6E−06	34	–
B3	2E−06 (1)	n. m.	n. m.	n. m.	n. m.	–
C1	4E−05 (7)	9E−05 (2)	2.1	5.9E−06	15	–
C2	2E−06 (1)	9E−05 (2)	42	3.1E−07	295	–
F1	3E−05 (1)	6E−05 (2)	1.7	–	–	–
All sites						S

absorption rate when the moisture volume is approaching its maximum capacity and/or when capillary water enters the BIRC. At the F1 site both shapes were concave.

The capillary absorption plots (amount of absorbed water over time) do not form straight lines, but instead form curves, and hence the w value (sometimes also referred as parameter C or CWA) cannot be obtained (cf., Siegesmund and Dürrast, 2011; Concha-Lozano et al., 2012). Instead of the w value, we list the Tx values (Eqs. (7), (8) in Supplementary material) for various fractions of capillary absorbed water in Table 10. To compare the capillary absorption rate via the BIRC and its subsurface, the values T20, T50, and T80 were used, which cover a considerable part of the capillary absorption range.

Table 10 shows that the capillary absorption ratio (via BIRC/via subsurface) is 3–9% in the case of the B1 site and 13–45% for other sites with a BIRC (T20–T80 values). As only one measuring via the BIRC and one measuring via its subsurface was performed for each study site, data from all the study sites were analyzed together. Capillary absorption via the BIRC is significantly reduced by a factor of 2–33 compared to its subsurface for T20, T50 and T80. For the F1 site, the capillary absorption ratio is 52–62%. Reduction by a factor of 2 in the case of F1 is probably caused by a thin film of fines coating the surface (see Supplementary material for more details).

4.3.4. Fluorescent dye experiments

BIRC hydrophobicity was clearly visualized and demonstrated by the experiments with fluorescein dye. In all cases, the penetration of the fluorescein dye through the subsurface parts of the cores was more or less uniform, while penetration through the BIRC was strongly retarded or even prohibited (Fig. 11). The highest hydrophobicity was found for the B1 and C2 cores, lower in the C1, and lowest for B2. The hydrophobic zone, where fluorescein dye did not penetrate, was 1–2 mm thick. In contrast, no hydrophobicity was observed in the case of the F1 core without a BIRC.

4.4. Observation of erosion patterns in quarry and on exposed cores

As observed at several sites in the quarry, surface erosion clearly propagates from the cliff tops downwards, and destroys the BIRC or its exposed subsurface (Figs. 1d 2a, b). Except for this uppermost destabilized zone, the BIRC surfaces are stable, and even all exposed surfaces after sampling cores were inhabited by a new BIRC in less than one year without traces of erosion. At the F1 site, the erosion under natural conditions is excluded, as this site is situated under an overhang, and unlike other sites, it is shielded from rain and the action of flowing water. The erosion rate of the surface lacking a BIRC was measured in the immediate surroundings of the B3 site, where eroded sand was collected over a 1 year period (in 2013). The surface erosion rate calculated to the real surface area (3D) was ~2 mm per year. As the material was very friable at the B3 site (locked sand), the erosion rate at other exposures in the surroundings of the studied sites are probably much lower.

The cores with BIRC left out in the open roof, exposed to rain and frost action, showed rapid erosion rates of several millimeters per month (Fig. 12). The B surfaces facing upward were destroyed by impacting rain droplets within 3 months (samples B1, B2). On the other hand, C surfaces facing upward resisted erosion for about six months, even to frost action, possibly due to their smoother surface. Steeply dipping surfaces resisted rain erosion well, except for the F1 sample without a BIRC. The B and C surfaces often peeled off from the inner sandstone and bent, demonstrating the important role of organic matter in their cohesion (Fig. 12c). After the decay of organic material in the spring, the surfaces were rapidly eroded. All F1 cores disintegrated within only two months (rain total = 110 mm), and their surfaces showed no resistance to erosion. The B2 core was the second most erodible, and lasted seven months (rain total = 260 mm; 39 freezing periods with a duration >12 h). The most durable (B1, C1, and C2) cores lasted up to 10 months, with rain totals of 360 mm, and 42 freezing periods.

Significance of all these observations is discussed together with other data in Section 5.3.

5. Discussion

5.1. Increase of mechanical resistance due to BIRC

Three independent techniques were used to compare the mechanical resistance of BIRC with its subsurface: (i) drilling resistance, which measures abrasivity; (ii) tensile strength (TSP), which measures the resistance to tensile force; and (iii) REI, a test of erodibility using a water jet. Each approach affects materials in very different way. Yet all methods yielded a distinct difference between the resistances of 10–50 year old BIRC and the subsurface sandstone. BIRC showed a significantly higher dry TSP at all but one site, and it showed significantly lower erodibility at all sites when compared to its subsurface. The

Table 9
Permeability of sandstone for water vapor. δ-water vapor diffusion coefficient, μ-water vapor resistance factor. Number of measurements is given in parentheses.

Site	Mean δ outer c. (s)	Mean δ inner c. (s)	Ratio δ (inner/outer)	Mean μ outer c.	Mean μ inner c.	Mean surface δ (s)	Ratio δ (subsurface/surface)	Significant difference of δ between surface/subsurface?
B1	2.2E−11 (1)	3.6E−11 (2)	1.6	8	5	5.3E−12	7	S
B2	2.4E−11 (2)	4.2E−11 (1)	1.8	7	4	4.9E−12	9	–
B3	3.0E−11 (1)	3.9E−11 (1)	1.3	6	4	1.1E−11	4	–
C1	2.9E−11 (2)	3.5E−11 (2)	1.2	6	5	1.0E−11	3	NS
C2	1.9E−11 (2)	2.0E−11 (2)	1.1	9	9	1.4E−11	1	NS
F1	4.9E−11 (3)	3.2E−11 (2)	0.7	5	5	–	–	–
All sites								NS

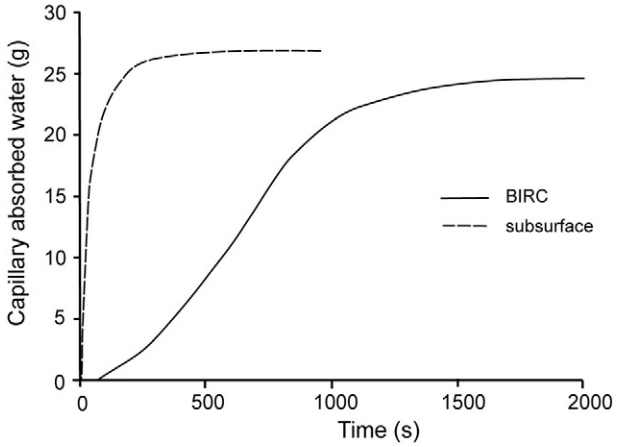

Fig. 10. Example of absorption curves (B1 site). If capillary water enters the core via the BIRC, the absorption curve is convex for most of the absorption capacity. For absorption via the subsurface, the absorption curve is concave. Absorption via the BIRC is significantly slowed down.

correspondence of the results of all methods clearly shows that BIRC is far more resistant than the original sandstone in the subsurface. Thus, only 10–50 year old BIRC is capable of protecting the underlying sandstone. To our knowledge, such a comparison had never been made before.

Some increase of mechanical resistance had already been found in the case of two year old BIRC; however, it is not comparable with the resistance of 10–50 year old BIRC (Tables 5, 7). This corresponds to the TOC content, which is also much lower in a two year old BIRC than in one that is 10–50 years old. These results are in agreement with study by Kurtz and Netoff (2001), who performed penetration tests on sand with and without a cultivated cyanobacterial biocrust (not on real sandstone). The experimental biocrust, unlike the sterile sand, was able to resist surface penetration using a light force penetrometer.

Additionally, surface F1, which can be considered as a BIRC-free "control" sample, does not show significantly increased mechanical resistance compared to its subsurface in any of the parameters measured. This is in good agreement with the results of tests on BIRC cores after the thermal removal of organic matter (calcination). Calcined BIRC shows similar or only a slightly higher mechanical resistance than does the subsurface. The difference between calcined BIRC and the subsurface could be caused by the presence of a small amount of mineral cement (clay) or by an abundance of fines in the BIRC. Nevertheless, a drastic decrease of mechanical resistance of the BIRC cores by removal of organic matter clearly demonstrates that organic matter is responsible for a dominant part of the mechanical resistance, while the contribution of inorganic hardening is of secondary importance. This is a novel finding, and mechanical testing of original vs. calcined cores can be a useful tool to determine the role of organic matter in the resistance of older case hardened surfaces in future studies.

It still remains to be answered whether the fungal hyphae are responsible for the increased mechanical resistance of the sandstone surface. An experiment with a zymolyase enzyme mixture, which decomposes fungal cell walls (Phalip et al., 2004), indicated that fungal hyphae contributed considerably to the mechanical resistance of the surface layer. The BIRC tested from both the B1 and B3 sites were weakened by the enzyme more than by the buffer alone, and also disintegrated significantly more when exposed to shaking after enzymatic digestion. This indicates that the BIRC is susceptible to an enzymatic agent, which specifically attacks fungal hyphae (Figs. S2 and S3 in Supplementary material). On optical microscope and SEM images it is evident that the BIRC, including the fungi hyphae, acts as a cohesion source (Fig. S2 in Supplementary material).

5.2. Effect of BIRC on capillary water and vapor transport

Saturated hydraulic conductivity (K), capillary water absorption, and the degree of fluorescent dye propagation were used as independent parameters to compare the flow of gravitational and capillary water via BIRC and the subsurface.

K was found to be significantly decreased by the BIRC compared to the original sandstone in the subsurface. This is consistent with other studies, where the decrease of K by biomass growth in a porous media is well-documented (Dennis and Turner, 1998; Thullner et al., 2002; Brovelli et al., 2009; Seifert and Engesgaard, 2012). Reduced K was reported on sandstone BIRC by Robinson and Williams (1987), but the measurements of BIRC and subsurface K were not done at the same location, which brings uncertainty into any comparison.

Similarly, the BIRC significantly reduces the rate of capillary water absorption compared to the original subsurface sandstone. A slight reduction was also found at the F1 site without BIRC, which is probably caused by a thin film of fines coating the surface. Low capillary absorption via the BIRC is predominantly caused by its hydrophobicity (Shirtcliffe et al., 2006; Hauck et al., 2008), as was also nicely demonstrated by the fluorescent dye experiments (Fig. 11). Capillary water absorption by sandstone is a frequently measured parameter (Meinhardt et al., 2012; Mol and Viles, 2012;). Reduction due to a crust was found on limestones (Török, 2003; Concha-Lozano et al., 2012), and on a lightweight aggregate by Bogas et al. (2015); however, we are unaware of any similar study on sandstone BIRC.

Conversely, the water vapor flux rate was not significantly affected by BIRC at all sites but one. While even a small amount of

Table 10
Capillary absorption values for different levels of absorption ($g\ m^{-2}\ s^{-1}$). Values of capillary absorption measured via the BIRC are in the numerator, those measured via the subsurface are in the denominator. The ratio of these two values is given as a percentage.

Site	T20	T50	T80	T100	Significant difference of capillary water absorption between surface/subsurface?
B1	6/191 (3%)	8/195 (4%)	9/105 (9%)	8/60 (13%)	–
B2	51/250 (20%)	39/266 (15%)	33/118 (28%)	14/32 (44%)	–
B3	46/179 (26%)	37/277 (13%)	29/120 (24%)	17/16 (106%)	–
C1	59/217 (27%)	23/79 (29%)	14/31 (45%)	8/11 (73%)	–
C2	59/254 (23%)	72/465 (15%)	41/199 (21%)	16/42 (38%)	–
F1	152/292 (52%)	88/147 (60%)	50/81 (62%)	34/51 (67%)	–
All sites					S

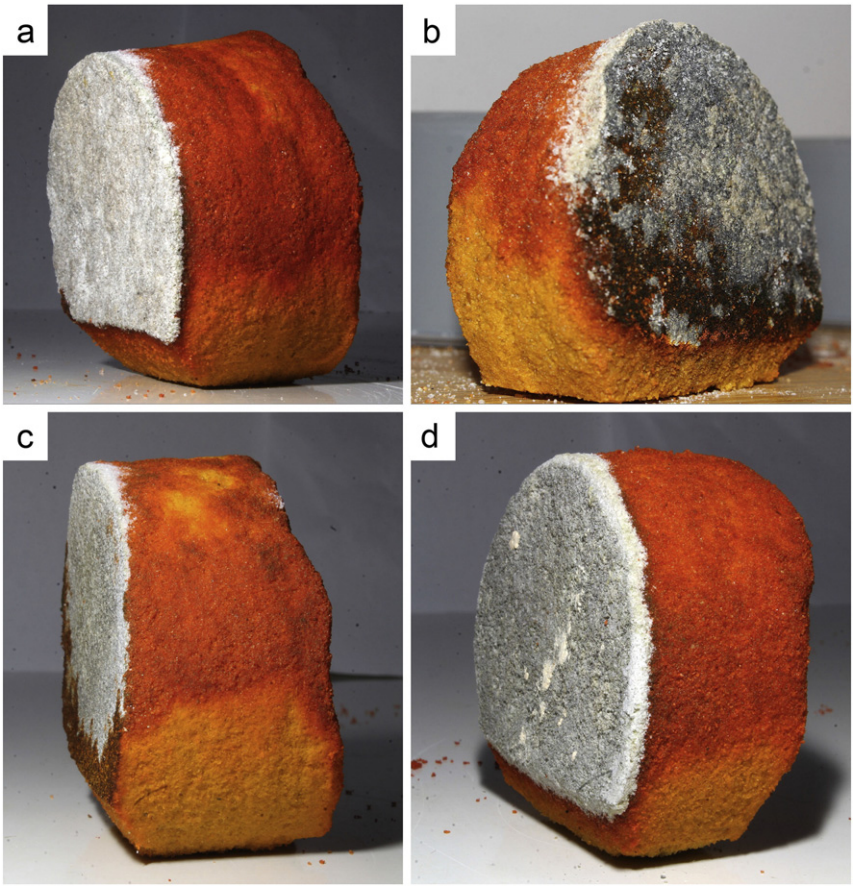

Fig. 11. Hydrophobicity of BIRC visualized by fluorescent dye propagation via the cores (see Fig. 5 for experimental setup); origin of cores: a) B1; b) B2; c) C1; d) C2 sites.

hydrophobic organic can greatly slow down the capillary water flow in the pores (Domenico and Schwartz, 1998), it seems that the hydrophobicity has only a small effect on water vapor diffusion. Several studies have dealt with vapor permeability of sandstone (e.g., Pavlík et al., 2008), but they did not compare BIRC with the subsurface.

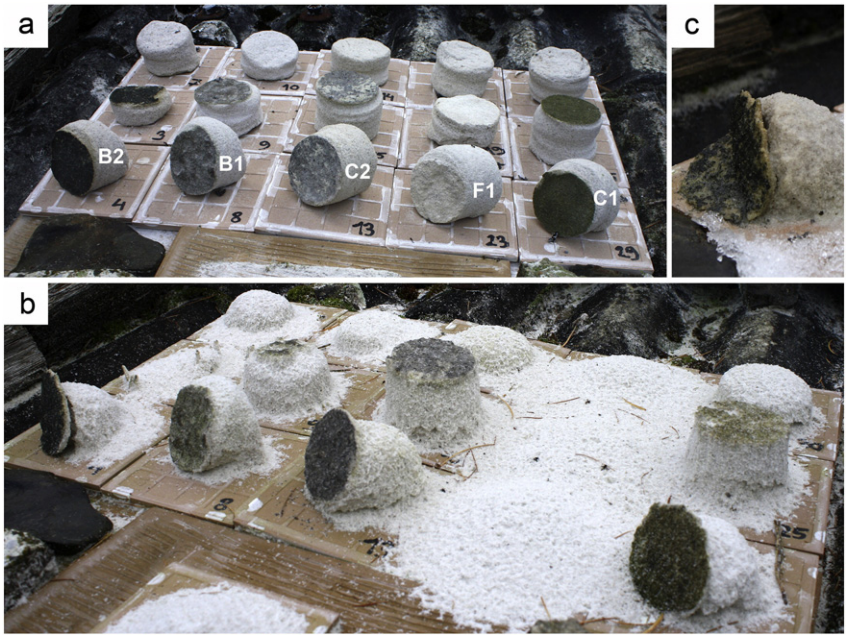

Fig. 12. Erosion experiment of drilled cores from different type of surfaces/sites (see white signs) exposed to natural climatic conditions. Orientation of the core surface (BIRC) is: subvertical in the front row; facing up in the middle row, and facing down in the back row. Situation at: a) The beginning 22.8.2014; b) At 14.12.2014. Part (c) shows a detail of the B2 core with deformed BIRC.

5.3. Other factors affecting the mechanical resistance of sandstone

The disparity between the results of the TSP and TS measurements (Section 4.2.2) were probably primarily caused by the different role of the interlocking of sand grains and gravity-induced stress in both measurements. TSP measures the tensile strength of small sandstone prisms with free sides, where the interlocking of grains and gravity-induced stress is minimized (Bruthans et al., 2014). The effect of the organic matter in the BIRC (the only remaining major cohesion source) is thus maximized in the TSP measurements, which results in the large contrast between the TSP of the BIRC vs. the subsurface, and also between the TSP of dry and wet samples. On the other hand, field TS measurements are strongly affected by gravity-induced stress in the sandstone massive, caused by the weight of the overburden and by the interlocking of the sand grains in the sandstone massive. These factors alone generate considerable resistance to tensile stress (Bruthans et al., 2014). The difference between the TS of the BIRC and the subsurface is thus diminished in a similar manner as the difference between relatively dry and wet surfaces.

Similarly, the rapid erosion of all cores left out in the open environment (Section 4.4) showed that sandstones from all sites, including the BIRC, are highly erodible if separated from their sandstone outcrop. This indicates that the most important stabilizing factor below the BIRC zone is gravity induced stress and interlocking of grains, which prevents or slows down dilatation of the pore space by erosion and weathering processes, such as the impacts of rain drops and the action of frost (Bruthans et al., 2014). The above-mentioned observations indicate that BIRC can only effectively stabilize a very surficial zone (a few millimeters thick). This seems to be sufficient to eliminate the erosion caused by raindrops and flowing water if the whole surface is covered by a BIRC, and the sandstone is in the form of a large outcrop (so it cannot easily dilate). Additional sources of stabilization (inorganic cement, gravity-induced stress, smooth surfaces disabling expansion of the pore space) are needed to protect the subsurface from disintegration by frost weathering and other processes occurring below the BIRC. If these additional sources of stabilization are missing, the BIRC will peel off by subsurface expansion, and the more erodible underlying material will be exposed. Exactly this process occurred in the uppermost portions of the B3, C1, and C2 sites, which lack gravity-induced stress (Figs. 1d, 2a, b).

Just as any chain will fail once its weakest link fails, the BIRC covered sandstone will erode if either the organic coating resistance will be exceeded or if any process (e.g., frost weathering) will destabilize the sandstone below the BIRC. Future studies should therefore not solely focus on BIRC, but also on those processes compromising the stability of the sandstone below the BIRC zone.

5.4. Role of BIRC on sandstone faces

The ability of biota to colonize sandstone surfaces within two years, and to fully protect surfaces in a few decades confirms the ideas of Arino et al. (1995) on the importance of bioprotection. Such a rate is much faster than development of mineral case hardening (Dorn et al., 2012). Thus, BIRC probably plays a primary role in stabilizing fresh surfaces of weak sandstone such as: scars after rock falls, artificial sandstone walls, road cuts, and other previously rapidly eroded areas. As BIRC development is limited by sufficient moisture content, environmental factors such as exposure to rain and sun radiation may via the occurrence of BIRC control the erosion rates of sandstone surfaces.

It is likely that with increased time the share of mineral case hardening acting on the resistance of BIRC is increasing, but there is currently a lack of data to support this idea. The role of organic matter in the mechanical resistance of case hardened sandstones is often neglected, while silica, iron and manganese oxides, gypsum, and clay minerals are believed to be the major hardening agents (Conca and Rossman, 1982; Robinson and Williams, 1987; Viles and Goudie, 2004; Young et al., 2009; Adamovič et al., 2011). Mechanical tests on hundreds to thousands of year-old BIRC surfaces are needed to evaluate the role of organics on such surfaces.

The hydrophobicity of the BIRC considerably decreases the entry of rainwater into the sandstone (Garcia-Vallés, 2003), which may decrease the moisture content of the sandstone; thus, decreasing the frost weathering rate as its intensity increases with moisture content (Hall, 1988). On the other hand, if the source of moisture from inside the rock prevails, the opposite effect may occur. Since moisture is critical for many weathering processes (Paradise, 2002; Mol and Viles, 2013), BIRC may have a large effect on these processes by retarding the moisture flux.

BIRC may also affect the evolution of microforms such as honeycombs. In the Bohemian Paradise of the Czech Republic, the honeycombed backwalls are often covered by BIRC, while the honeycomb's lips are bare (Adamovič et al., 2006), which may affect the capillary moisture flux on the microscale, and in turn affect the form evolution in some kind of feedback loop.

6. Conclusions

A wide set of techniques were applied in order to characterize the role of biologically-initiated rock crust (BIRC) on relatively young surfaces of friable sandstone. Together with the BIRC, the subsurface zone of the sandstone was studied, and the data collected from both environments were carefully evaluated. The BIRC studied, of various ages, were 2–6 mm thick and are macroscopically recognizable as a hardened zone with a greenish to grayish color on their surface. Besides the organic matter, mostly formed by various fungi and green algae, the BIRC is enriched in kaolinite, clay-to-silt-sized quartz particles, and atmospheric dust particles.

Our measurements clearly show that the studied BIRC significantly changes the mechanical and hydraulic properties of young sandstone surfaces. It effectively protects the surface from erosion via both an increase of tensile strength and resistance to abrasion. The BIRC also markedly reduces saturated hydraulic conductivity and capillary water absorption, which significantly alters both the infiltration and evaporation rates, and thus affects most of the processes controlled by moisture content and flux. However, the presence of a BIRC has no measurable influence on the diffusion of water vapor.

Mechanical tests performed after removing the organic matter clearly demonstrated that the organic matter in the BIRC is the major source for the increased resistance to erosion. Thus, the effect of the mineral cement is minor in young BIRC. This explains why BIRC can successfully protect surfaces that are only a few years old from raindrops and the erosion of flowing water.

While the BIRC only stabilizes the near-surface zone of the sandstone, additional sources of stabilization such as gravity-induced stress, interlocking of grains, and inorganic cement contribute to the resistance of the deeper subsurface zone to weathering by frost action and other processes. Therefore, the protective effect of the BIRC should always be considered together with the stability of the sandstone below the BIRC - i.e., stability of the entire landform.

This study demonstrated very clearly that “pioneer” organisms are capable of inhabiting and protecting freshly exposed sandstone surfaces within two years. Thus, BIRC may represent a prime step for the development of a more complex rock induration, including inorganic cements such as case hardening. However, more detailed studies focused on the gradual formation and time evolution of such phenomena are needed.

Supplementary data to this article can be found online at http://dx.doi.org/10.1016/j.geomorph.2016.09.040.

Acknowledgments

This research was funded by the Czech Science Foundation (GA CR No. 13-28040S and 16-19459S), and Grant Agency of Charles University

(No. 386815). The research was also supported by Institutional Research Plans RVO 67985831 and 67985891. A number of colleagues helped with the laboratory and analytical work: A. Kobrlová and P. Škaloud from Charles University (hydraulic conductivity measurements, cultivation and identification of algae), O. Benada and Z. Večerková from the Institute of Microbiology CAS (staining the samples with Pb citrate), and R. Fabeš from the Institute of Theoretical and Applied Mechanics CAS (drilling resistance measurements). We would like to express our sincere thanks to Sklopísek Střeleč, a.s., namely to Lukáš Horák and managing director Petr Hübner for admission to the quarry. The authors are grateful to three anonymous reviewers and to the handling editor S. Lecce for their constructive criticisms which helped to significantly improve the manuscript.

References

Adamovič, J., Mikuláš, R., Cílek, V., 2006. Sandstone districts of the Bohemian Paradise: emergence of a romantic landscape. Geolines 21, 1–100.
Adamovič, J., Mikuláš, R., Schweigstillová, J., Böhmová, V., 2011. Porosity changes induced by salt weathering of sandstones, Bohemian Cretaceous Basin, Czech Republic. Acta Geodyn. Geomater. 8 (1), 29–45.
Ahmadjian, V., 1993. The Lichen Symbiosis. John Wiley and Sons, New York, pp. 1–6.
Arino, X., Ortega-Calvo, J.J., Gomez-Bolea, A., Saiz-Jimenez, C., 1995. Lichen colonization of the Roman pavement at Baelo Claudia (Cadiz, Spain): biodeterioration vs. bioprotection. Sci. Total Environ. 167, 353–363.
Bellinzoni, A.M., Caneva, G., Ricci, S., 2013. Ecological trends in travertine colonization by pioneer algae and plant communities. Int. Biodeterior. Biodegrad. 51, 203–210.
Bjelland, T., Thorseth, I.H., 2002. Comparative studies of the lichen-rock interface of four lichens in Vingen, western Norway. Chem. Geol. 192, 81–98.
Bogas, J.A., Gomes, M.G., Real, S., 2015. Capillary absorption of structural lightweight aggregate concrete. Mater. Struct. 48 (9), 2869–2883.
Brehm, U., Gorbushina, A., Mottershead, D., 2005. The role of microorganisms and biofilms in the breakdown and dissolution of quartz and glass. Palaeogeogr. Palaeoclimatol. Palaeoecol. 219, 117–129.
Brovelli, A., Malaguerra, F., Barry, D.A., 2009. Bioclogging in porous media: model development and sensitivity to initial conditions. Environ. Model. Softw. 24, 611–626.
Bruthans, J., Světlík, D., Soukup, J., Schweigstillová, J., Válek, J., Sedlackova, M., Mayo, A.L., 2012. Fast evolving conduits in clay-bonded sandstone: characterization, erosion processes and significance for origin of sandstone landforms. Geomorphology 177–178, 178–193.
Bruthans, J., Soukup, J., Vaculikova, J., Filippi, M., Schweigstillova, J., Mayo, A.L., Masin, D., Kletetschka, G., Rihosek, J., 2014. Sandstone landforms shaped by negative feedback between stress and erosion. Nat. Geosci. 7, 597–601.
Büdel, B., Weber, B., Kühl, M., Pfanz, H., Sültemeyer, D., Wessels, D., 2004. Reshaping of sandstone surfaces by cryptoendolithic cyanobacteria: bioalkalization causes chemical weathering in arid landscapes. Geobiology 2, 261–268.
Chen, J., Blume, H.P., Beyer, L., 2000. Weathering of rocks induced by lichen colonization – a review. Catena 39, 121–146.
Conca, J.L., Rossman, G.R., 1982. Case hardening of sandstone. Geology 10, 520–523.
Concha-Lozano, N., Gaudon, P., Pages, J., de Billerbeck, G., Lafon, D., Eterradossi, O., 2012. Protective effect of endolithic fungal hyphae on oolitic limestone buildings. J. Cult. Herit. 13, 120–127.
Cutler, N.A., Viles, H.A., Ahmad, S., McCabe, S., Smith, B.J., 2013. Algal greening and the conservation of stone heritage structures. Sci. Total Environ. 442, 152–164.
Dade, W.B., Davis, J.D., Nichols, P.D., Nowell, A.R.M., Thistle, D., Trexler, M.B., White, D.C., 1990. Effects of bacterial exopolymer adhesion on the entrainment of sand. Geomicrobiol J. 8, 1–16.
Dennis, M., Turner, J., 1998. Hydraulic conductivity of compacted soil treated with biofilm. J. Geotech. Geoenviron. 24, 120–127.
Domenico, P.A., Schwartz, F.W., 1998. Physical and Chemical Hydrologeology. 2nd ed. John Wiley and Sons, Inc., New York 506 pp.
Dorn, R.I., Dorn, J., Harrison, E., Gutbrod, E., Gibson, S., Larson, P., Cerveny, N., Lopat, N., Groom, K.M., Allen, C.D., 2012. Case hardening vignettes from the western USA: convergence of form from a divergence of hardening processes. Assoc. Pac. Coast Geogr. Yearb. 74, 1–12.
Friedmann, E.I., 1982. Endolithic microorganisms in the Antarctic Cold Desert. Science 215, 1045–1053.
Garcia-Vallés, M., 2003. Lichenic growth as a factor in the physical deterioration or protection of Cappadocian monuments. Environ. Geol. 43, 776–781.
Goloubic, S., Friedmann, I., Schneider, J., 1981. The lithobiontic ecological niche, with special reference to microorganisms. J. Sediment. Petrol. 51, 475–478.
Gómez-Alarcón, G., Muñoz, M., Ariño, X., Ortega-Calvo, J.J., 1995. Microbial communities in weathered sandstones: the case of Carrascosa del Campo church, Spain. Sci. Total Environ. 167, 249–254.
Gorbushina, A.A., 2007. Life on the rocks. Environ. Microbiol. 9 (7), 1613–1631.
Grondona, I., Monte, E., Rives, V., Vicente, M.A., 1997. Lichenized association between *Septonema tormes* sp. nov., a cocoid cyanobacterium and green alga with unforeseen biopreservation effect of Villamayor sandstone at Casa Lis of Salamanca, Spain. Mycol. Res. 101, 1489–1495.
Hall, K., 1988. A laboratory simulation of rock breakdown due to freeze-thaw in a maritime Antarctic environment. Earth Surf. Process. Landf. 13, 369–382.
Hallmann, C., Stannek, L., Fritzlar, D., Hause-Reitner, D., Friedl, T., Hoppert, M., 2013. Molecular diversity of phototrophic biofilms on building stone. FEMS Microbiol. Ecol. 84, 355–372.
Hauck, M., Jurgens, S.R., Brinkmann, M., Herminghaus, S., 2008. Surface hydrophobicity causes SO_2 tolerance in lichens. Ann. Bot. 101, 531–539.
Hauser, M., Čtyroký, V., Krutský, N., Macková, E., Bylová, I., 1965. Střeleč. Surovina: sklářské a slévárenské písky. Geoindustria, Praha. Geofond No. FZ004733. Geoindustria, Czech.
Heinrichs, K., 2008. Diagnosis of weathering damage on rock-cut monuments in Petra, Jordan. Environ. Geol. 56, 643–675.
Hirsch, P., Eckhardt, F.E.W., Plamer, R.J., 1995. Methods for the study of rock-inhabiting microorganisms – a mini review. J. Microbiol. Methods 23, 143–167.
Käss, W., 1998. Tracing Technique in Geohydrology. Balkema, Rotterdam 581 pp.
Kidron, G.J., 1999. Differential water distribution over dune slopes as affected by slope position and microbiotic crust, Negev Desert, Israel. Hydrol. Process. 13, 1665–1682.
Kurtz, H.D., Netoff, D.I., 2001. Stabilization of friable sandstone surfaces in a desiccating, wind-abraded environment of south-central Utah by rock surface microorganisms. J. Arid Environ. 48, 89–100.
Langhans, T.M., Storm, C., Schwabe, A., 2009. Community assembly of biological soil crusts of different successional stages in a temperate sand ecosystem, as assessed by direct determination and enrichment techniques. Microb. Ecol. 58, 394–407.
Lisci, M., Monte, M., Pacini, E., 2003. Lichens and higher plants on stone: a review. Int. Biodeterior. Biodegrad. 51, 1–17.
Martínková, N., Horáček, I., Bačkor, P., Bartonička, T., Blažková, P., Červený, J., Falteisek, L., Gaisler, J., Hanza, V., Horáček, D., Hubálek, Z., Jahelková, H., Kolařík, M., Korytár, L., Kubátová, A., Lehotská, B., Lehotský, R., Lučan, R.K., Májek, O., Matějů, J., Řehák, Z., Šafář, J., Tájek, P., Tkadlec, E., Uhrin, M., Wagner, J., Weinfurtová, D., Zima, J., Zukal, J., Horáček, I., 2010. Increasing incidence of *Geomyces destructans* fungus in bats from the Czech Republic and Slovakia. PLoS One 5 (11), e13853.
Meinhardt, J., Snethlage, R., Auras, M., 2012. Natural stone monitoring – investigation methods for a reliable evaluation of the effectiveness of conservation measures. Proceedings of the 12th International Conference on the Deterioration and Conservation of Stone. Columbia University, New York City.
Mikuláš, R., 1999. Subaerial animal and plant bioerosion in sandstone castellated rocks (Pleistocene to Recent, Czech Republic). Bull. Geol. Soc. Den. 45, 177–178.
Mol, L., Viles, H.A., 2012. The role of rock surface hardness and internal moisture in Tafoni development in sandstone. Earth Surf. Process. Landf. 37 (3), 301–314.
Mol, L., Viles, H.A., 2013. Exposing drying patterns: using electrical resistivity tomography to Monitr capillary rise in sandstone under varying drying conditions. Environ. Earth Sci. 68, 1647–1659.
Pamplona, M., Kocher, M., Snethlage, R., Aires-Barros, L., 2007. Drilling resistance: overview and outlook. Z. Dtsch. Ges. Geowiss. 158 (3), 665–676.
Paradise, T.R., 1997. Disparate sandstone weathering beneath lichens, red mountain, Arizona. Geogr. Ann. Ser. B 79 (3), 177–184.
Paradise, T.R., 2002. Sandstone weathering and aspect in Petra, Jordan. Z. Geomorphol. 46, 1–17.
Pavlík, Z., Michálek, P., Pavlíková, M., Kopecká, I., Maxová, I., 2008. Water and salt transport and storage properties of Mšené sandstone. Constr. Build. Mater. 22 (8), 1736–1748.
Phalip, V., Hatsch, D., Jeltsch, J.M., 2004. Application of a yeast method for DNA extraction associated with database interrogations for the characterization of various filamentous fungi from diseased hop. Biotechnol. Lett. 26, 409–413.
Pointing, S.B., Belnap, J., 2012. Microbial colonization and controls in dryland systems. Nat. Rev. Microbiol. 10 (8), 551–562.
Reynolds, E.S., 1963. The use of lead citrate at high pH as an electron-opaque stain in electron microscopy. J. Cell Biol. 17 (1), 208–212.
Robinson, D.A., Williams, R.B.G., 1987. Surface crusting of sandstones in southern England and northern France. In: Gardiner, V. (Ed.), International Geomorphology 1986 Part II. Wiley and Sons, London, pp. 623–635.
Robinson, D.A., Williams, R.B.G., 2000. Accelerated weathering of a sandstone in the high atlas mountains of Morocco by an epilithic lichen. Z. Geomorphol. 44 (4), 513–528.
Seifert, D., Engesgaard, P., 2012. Sand box experiments with bioclogging of porous media: hydraulic conductivity reductions. J. Contam. Hydrol. 136–137, 1–9.
Shirtcliffe, N.J., Pyatte, F.B., Newten, M.I., McHale, G., 2006. A lichen protected by a superhydrophobic and breathable structure. J. Plant Physiol. 163, 1193–1197.
Siedel, H., Pfefferkorn, S., Plehwe-Leisen, E., Leisen, H., 2010. Sandstone weathering in tropical climate: results of low-destructive investigations at the temple of Angkor Wat., Cambodia. Eng. Geol. 115, 182–192.
Siegesmund, S., Dürrast, H., 2011. Physical and mechanical properties of rocks. In: Siegesmund, S., Snethlage, R. (Eds.), Stone in Architecture – Properties, Durability, 4th ed Springer, pp. 97–226.
Smits, M.M., Herrmann, A.M., Duane, M., Duckworth, O.W., Bonneville, S., Benning, L.G., Lundström, U., 2009. The fungal-mineral interface: challenges and considerations of micro-analytical developments. Fungal Biol. Rev. 23, 122–131.
Souza-Egipsy, V., Wierzchos, J., Sanco, C., Belmonte, A., Ascaso, C., 2004. Role of biological soil crust cover in bioweathering and protection of sandstones in a semi-arid landscape (Torrollones de Gabarda, Huesca, Spain). Earth Surf. Process. Landf. 29, 1651–1661.
Thullner, M., Zeyer, J., Kinzelbach, W., 2002. Influence of microbial growth on hydraulic properties of pore networks. Transp. Porous Media 49, 99–122.
Török, Á., 2003. Surface strength and mineralogy of weathering crusts on limestone buildings. Budapest Build. Environ. 38 (9), 1185–1192.

Uličný, D., 2001. Depositional systems and sequence stratigraphy of coarse-grained deltas in a shallow-marine, strike-slip setting: the Bohemian Cretaceous Basin, Czech Republic. Sedimentology 48, 599–628.
Viles, H.A., Goudie, A.S., 2004. Biofilms and case hardening on sandstones from Al-Quwayra, Jordan. Earth Surf. Process. Landf. 29, 1473–1485.
Warren, S.D., 1995. Ecological role of microphytic soil crusts in arid ecosystems. In: Allsopp, D., Hawksworth, D.L., Colwell, R.R. (Eds.), Microbial Diversity and Ecosystem Function. Cab International, London, pp. 199–209.
Warscheid, T., Braams, J., 2000. Biodeterioration of stone: a review. Int. Biodeterior. Biodegrad. 46, 343–368.
Wessels, D., Venter, D., Wessels, W., Wessels, L., 1995. Experimental strain analysis of Clarens Sandstone colonized by endolithic lichens. Koedoe 38 (2), 35–47.
Young, R.W., Wray, R.A.L., Young, A.R.M., 2009. Sandstone landforms. Cambridge University Press, Cambridge, pp. 1–304.